GEOPHYSICAL AND GEOCHEMICAL CHARACTERIZATION AND DELINEATION OF A CRUDE OIL SPILL IN A HIGHLY SALINE ENVIRONMENT

By

CAMERON STUART ROSS

Bachelor of Science in Geology

Grand Valley State University

Allendale, Michigan

2008

Submitted to the Faculty of the
Graduate College of the
Oklahoma State University
in partial fulfillment of
the requirements for
the Degree of
MASTER OF SCIENCE
May, 2013

GEOPHYSICAL AND GEOCHEMICAL

CHARACTERIZATION AND DELINEATION OF A

CRUDE OIL SPILL IN A HIGHLY SALINE

ENVIRONMENT

Thesis Approved:

Dr. Estella Atekwana

Thesis Adviser

Dr. Eliot Atekwana

Dr. Todd Halihan

.

ACKNOWLEDGEMENTS

I would like to thank my advisors Dr. Estella Atekwana, Dr. Eliot Atekwana, and Dr. Todd Halihan for their guidance, patience, mentorship, and friendship throughout my Master's program at Oklahoma State University.

I would also like to thank Dr. Dale Werkema from the U.S. Environmental Protection Agency. The opportunity you gave me to work for you and the Agency was invaluable regarding both experience and financially. Additionally the time, effort, and patience you showed me through the research process is greatly appreciated. This work was funded partially by the U.S. Environmental Protection Agency Office of Research and Development student services contract number EP-11-D000452. This project was also partially funded by National Science Foundation RAPID Award OCE-1049301.

My gratitude goes out to Dr. Lee Slate, Dr. Dimitrios Ntatlagiannis, Dr. Babu Fathepure, Jeffery Heenan, Michael Bacon, Sen Wei, and James Nolan, and Malachi Lopez for their assistance in data collection, data processing, mentorship, and friendship.

Last by not least, I thank my family and friends for the guidance, support, and prayers. Most importantly Kathryn, I cannot express my gratitude for the sacrifices you have made, the encouragement you gave, and the never-ending support, you are my rock.

Name: Cameron Stuart Ross

Date of Degree: MAY, 2013

Title of Study: GEOPHYSICAL AND GEOCHEMICAL CHARACTERIZATION AND DELINEATION OF A CRUDE OIL SPLL IN A HIGHLY SALINE ENVIRONMENT

Major Field: Geology

Abstract: Geophysical and geochemical methods were used at Grand Terre 1 (GT1) Island off the coast of Louisiana, an island that had been heavily contaminated with crude oil associated with the April 2010 BP Deepwater Horizon oil spill.

Electrical methods and aqueous geochemistry have proven sensitive in the detection of contaminates, as well as the biological and chemical processes associated with the biodegradation of hydrocarbons in the subsurface. However, to the author's knowledge, all of these studies have dealt with mature (or aged) spills within a freshwater environment. The BP Deepwater Horizon oil spill therefor provided a unique opportunity to not only use traditional geophysical and geochemical methods to characterize and delineate fresh crude oil in a highly saline environment and to capture the early time biogeophysical signals resulting from the physical, chemical, and microbial transformation of crude oil in a highly saline environment.

Electrical resistivity and electromagnetic methods were used. Barometric pressure, temperature, electrical conductivity, and water level values for the shallow groundwater were continuously logged. Geochemical analysis was performed on water samples collected from piezometers networks installed in the impacted, transitional, and background areas. Sediment cores were retrieved throughout the site and used for grain size analysis, magnetic susceptibility, total organic and inorganic carbon, and x-ray fluorescence. Soil samples were collected for microbial analyses from the impacted and background areas. Microcosms were set up to determine the microbial diversity analysis was used to determine microbial community composition, and biodegradation potential of indigenous populations.

Based on the geochemical, microbial, and soil analysis, the relatively higher apparent resistivity anomaly observed between the depths of 0.20 m to 1.20 m bgs could be explained by two scenarios(1): elevated resistivity was caused by gas in the subsurface produced by the degradation of organic matter coupled to sulfate and iron reduction. (2): from variations in salinity. This research demonstrates the sensitivity of geophysical and geochemical methods commonly used to detect contaminates in freshwater environment can also be utilized in a saline, coastal environment.

TABLE OF CONTENTS

LIST OF TABLES

Table Page

LIST OF FIGURES

Figure Page

CHAPTER I

INTRODUCTION

1.1 Problem Statement

Crude oil regularly escapes into the environment during extraction, transportation, and while in storage. The final destination of many of these contaminants will be the infiltration into a freshwater aquifers. The potential contamination of aquifers has been a primary driving force behind the extensive research in the detection and characterization of non-aqueous phase liquids (NAPL) using geophysical, chemical, and biological methods. While the field locations for this branch of research are globally diverse, most of this research to date has been conducted in a freshwater environment characterizing weathered or mature oil (where the contamination has been in existence for decades). In the last 15 years ~ 2.25 billion liters (CEDRE, 2012) of crude oil have been spilled near a salt water coast line impacting coastal aquifers and wetlands. The two worst oil spills in United State history: the *Exxon Valdez* spill in 1989 off the coast of Prince William Sound, Alaska and the BP *Deepwater Horizon* spill in 2010 in the Gulf of Mexico released a total over 870 thousand liters of crude oil.

The characteristic geophysical response of hydrocarbon-contaminated media has been attributed to a variety of physical, chemical, and biological mechanisms (Che-Alota et al., 2009). The anomalous increase in the bulk electrical conductivity of areas contaminated with NAPL has been extensively researched) using electrical methods to characterize the extent of contamination

(e.g., Sauck et al., 1998; Atekwana et al., 2000; Werkema et al., 3003; Atekwana et al., 2004a, b, and c; Atekwana et al., 2005, Benson et al., 1997; Halihan et al., 2005; Kaugmann and Deceuster, 2007; Yang et al., 2007). Electrical methods in particular are sensitive to variable changes in soil properties, including the nature of the solid constituents, and of voids, degree of water saturation, electrical resistivity of the fluid (chemistry of the pore fluid), and temperature (Archie, 1942; Samouëlian et al., 2005). All of the variables previously mentioned have been shown to be influenced by biologic activity adding to the complexity of the subsurface environment. Geophysical studies suggest the weathering of aquifer solids by the organic and carbonic acids produced during biodegradation results in an increase in the concentration of dissolved solutes which increase the bulk electrical conductivity (Sauck et al., 2000, Atekwana et al., 2000).

A conceptual model of petroleum hydrocarbon contamination developed by Che-Alota et al. (2009) illustrates the temporal behavior of bulk electrical conductivity from contaminant mass reduction by biodegradation, natural attenuation, or potentially engineered remediation (Figure 1). Although Che-Alota et al., (2009) uses bulk conductivity in their model to represent the geophysical response, the trend is valid for the application of either electrical resistivity (ER) or electromagnetic (EM) to hydrocarbon contamination. Figure 1 suggests multiple stages in the breakdown of hydrocarbons by microbial activity with coincident geophysical response: the first stage (Stage A) displays a decrease in the bulk conductivity relative to uncontaminated background due to the high electrical resistivity of the fresh petroleum hydrocarbon (Yang et al., 2007). However, over time, the excess organic carbon is expected to stimulate the activity of indigenous microorganism that breakdown the hydrocarbons producing a variety of metabolic byproducts such as organics acids and CO_2 (Baedecker et al., 1993; Bennett et al., 1996). The organic acids and carbonic acids result in enhanced mineral weathering (Stage B), releasing ions into solution and elevating the pore fluid conductivity. The end result is an enhancement of the

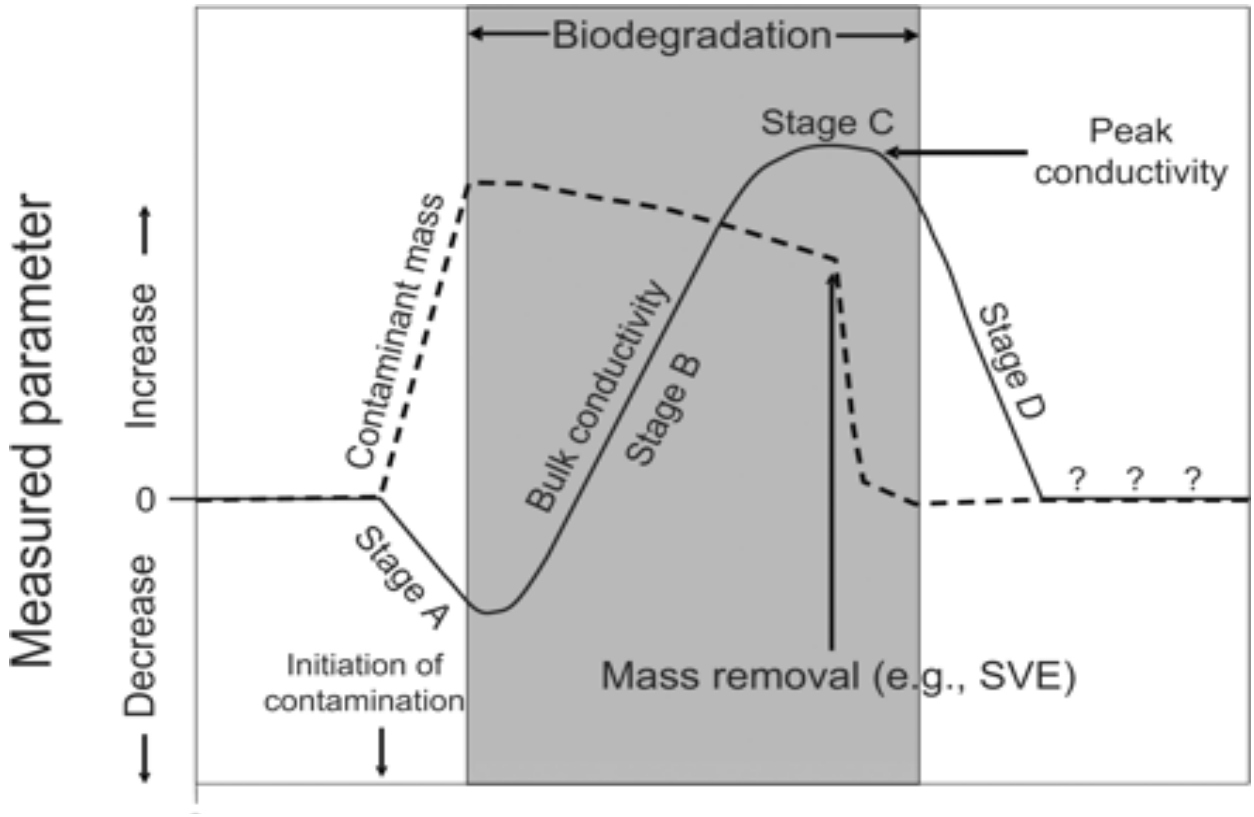

Figure 1. Conceptual model of the temporal bulk conductivities of behavior petroleum hydrocarbon due to contaminant mass reduction by natural attenuation, biodegradation, or engineered remediation. (Adapted from Che-Alota, 2009)

bulk electrical conductivity (Sauck, 2000; Atekwana et al., 2004a; Atekwana et al., 2004c; Atekwana et al., 2004d). As time progresses, the availability of terminal electron acceptors, organic-carbon-source concentration, and the microbial activity determines the reaction rate and production of ions in solution that contribute to the peak value of the bulk conductivity (Stage C). With the continuous removal of the contaminant masses by natural attenuation or engineered intrinsic remediation, Che-Alota et al. (2009) predicts a decrease in microbial activity and therefore a decrease in the bulk electrical conductivity to values close to pre-spill conditions (Stage D). It is important to note that the temporal frame required for these changes to occur depends on several factors, including the type and volume of hydrocarbon contamination, relative ease of contaminant degradation, presence of indigenous microorganisms, availability of terminal electron acceptors, as well as both the hydrology and hydrogeology of the site.

The application of the same geophysical technique at different sites, and even at different locations on the same site can produce dramatically different results (Atekwana and Atekwana, 2010). Che-Alota et al. (2009) model has been repeatedly enforced by past and current geophysical research. However, as previously stated, little to no research has been done in a saline environment that could be applied to this model. The BP *Deepwater Horizon* oil spill provided an unprecedented opportunity to characterize and delineate the crude oil in a saline environment. The study objective was to capture the early time biogeophysical signals resulting from the physical, chemical, and microbial degradation of the crude oil in a highly saline environment, thus describe the evolution of biogeophysical signals from a young to more mature crude spills. In this study, we interpret the geophysical results within the constraints of the biological and geochemical data acquired in order to better understand the geophysical signature of a fresh crude oil in a saline environment.

1.2 Site History

On April 20, 2010, oil and gas escaped from BP's *Deepwater Horizon* exploratory Macondo well located 130 miles to the SE of the southern tip of the Mississippi Delta (Operational Science Advisory Team. 2011). The blowout prevention (BOP) device at the well head and all the emergency shut-off equipment failed leading to the largest marine oil spill in the United States' history (Operational Science Advisory Team. 2011). The Nation Incident Command's Flow Rate Technical Group (FRTG) estimated 4.1 million barrels of oil were released into the water column and 2.1 million gallons of dispersants were applied at the ocean surface and wellhead (Operational Science Advisory Team. 2011). The FRTG Oil Budget calculator estimated that by July 14, 2010, an expected 17% was captured, 13% was naturally dispersed, 23% was evaporated or dissolved, 16% was chemically dispersed, 5% was burned, 3% was skimmed, and 23% was considered "remaining oil" either at the surface as light sheen or weathered tar balls, has been biodegraded, or has already come ashore (FRTG).

Crude oil began washing up on the beaches of Gulf Islands on June 1, 2010. By June 4 oil had been sited on 125 miles of Louisiana coast, and began washing up along Mississippi and Alabama barrier islands (Operational Science Advisory Team. 2011). In early July 2010, the first physical evidence of crude oil began to be seen in the form of tar balls washing up on the shores of Grand Isle, Louisiana (Operational Science Advisory Team. 2011). Remediation efforts provided by BP on the shores of Grand Isle and Grand Terra consisted of spatial delineation of the crude oil by auguring holes ~100m apart and marking if any crude oil was visible in the soil till. This was followed by separating the visually contaminated sediment from the uncontaminated either by shovel or by mechanical sifting equipment and shipping it off to be decontaminated.

Water sampling preformed at Grand Isle, LA by Allan et al. (2012) measuring the fraction of hydrophobic organic contaminants such as polycyclic aromatic hydrocarbons (PAHs).

Samplers were in the water column during heavy shoreline oiling in the month of June. Followed by a sharp decrease in concentration during August and September and the measurements had approximately returned to pre-oil spill concentrations by March 2011.

While spilled oil does naturally disperse in the coastal environment by storms and currents, chemical dispersants (such as Corexit 9500 and Dispersit SPC1000 used in the Deepwater Horizon spill are commonly used to accelerate the dispersal process. With respect to the remediation at the Deepwater Horizon site, these dispersants were initially sprayed directly on the surface of water over the well head by military aircrafts (Operational Science Advisory Team. 2011). This was followed by directly injecting the dispersant at the wellhead end of the riser pipe at a water depth of 1500 m in an attempt to prevent large slicks from forming directly at the surface above the wellhead and to reduce the magnitude of oil to impact the shoreline (Operational Science Advisory Team. 2011). The dispersant was injected into the deep-sea at high pressure and temperature causing physical dispersion and the creation of two zones with the highest concentrations of oil (Atlas and Hazen, 2011). Large droplets of oil floated to the surface while droplets between 10 and 60 μm were neutrally buoyant and were picked up by the current between the depths of 900 and 1300 m creating a suspended "cloud" of crude oil (Camilli et al., 2010).

1.3 Selection of Field Site

Maps on the website: Geoplatform.gov/gulfresponse (generated using data collected by NOAA (Figure 2)) showing the areas which had the highest recorded levels of crude oil impact were updated daily by NOAA. According to these maps, barrier islands in southern Louisiana (located ~ 180 miles to the NW of the blowout) Grand Isle, Grand Terre 1 (GT1), and Grand Terre 2 (GT2) was shown to be some of the most heavily impacted shores throughout the entire Gulf coast. It was discovered that GT1 to be a state protected wildlife reserve and therefore did not permit public access, making it the ideal site to install geophysical and geochemical

instrumentation required for the long term monitoring aspect of this research. A low lying area approximately 75 m from shore in the NE corner of GT1 was visually darker than any other area on the beach and was thought to be due to contamination. This area is referred to as the Elevated Resistivity Area (ERA) (Figure 3). A vegetative berm began 20 m from the westerly edge of the ERA; the area between the edges of the impacted zone to the berm is designated the transitional zone. The background zone is located an additional 60 m to the southwest of the transition zone in a sandy clearing within the vegetation.

1.4 Geology, Hydrology and Climate

GT1 is a barrier island composed entirely of sediments, most of which are terrigenous. Surface sediments of the island are primarily fine- to very fine-grained sand, some silt and with some clay.

The hydrographical network of the site is most influenced by the Gulf of Mexico and the Mississippi River to the East. In addition, there are small isolated bodies of water within the island that act as hyper-saline pools due to ocean water washing in coupled with partial evaporating.

The distribution of rainfall is characterized by highest values during the hurricane season of July and August with lows during May and November. The annual precipitation averages around 1600 mm. The climate is humid, mesothermic. Seasonal tide is characterized by a gradual increase starting in January and ending with the highs in the months of July, August, and September. Followed by a very sharp fall in sea level till January and the tides start the cycle again. The total change in the height of the sea level in reference to maximum sea level (MSL) is approximately 45 cm

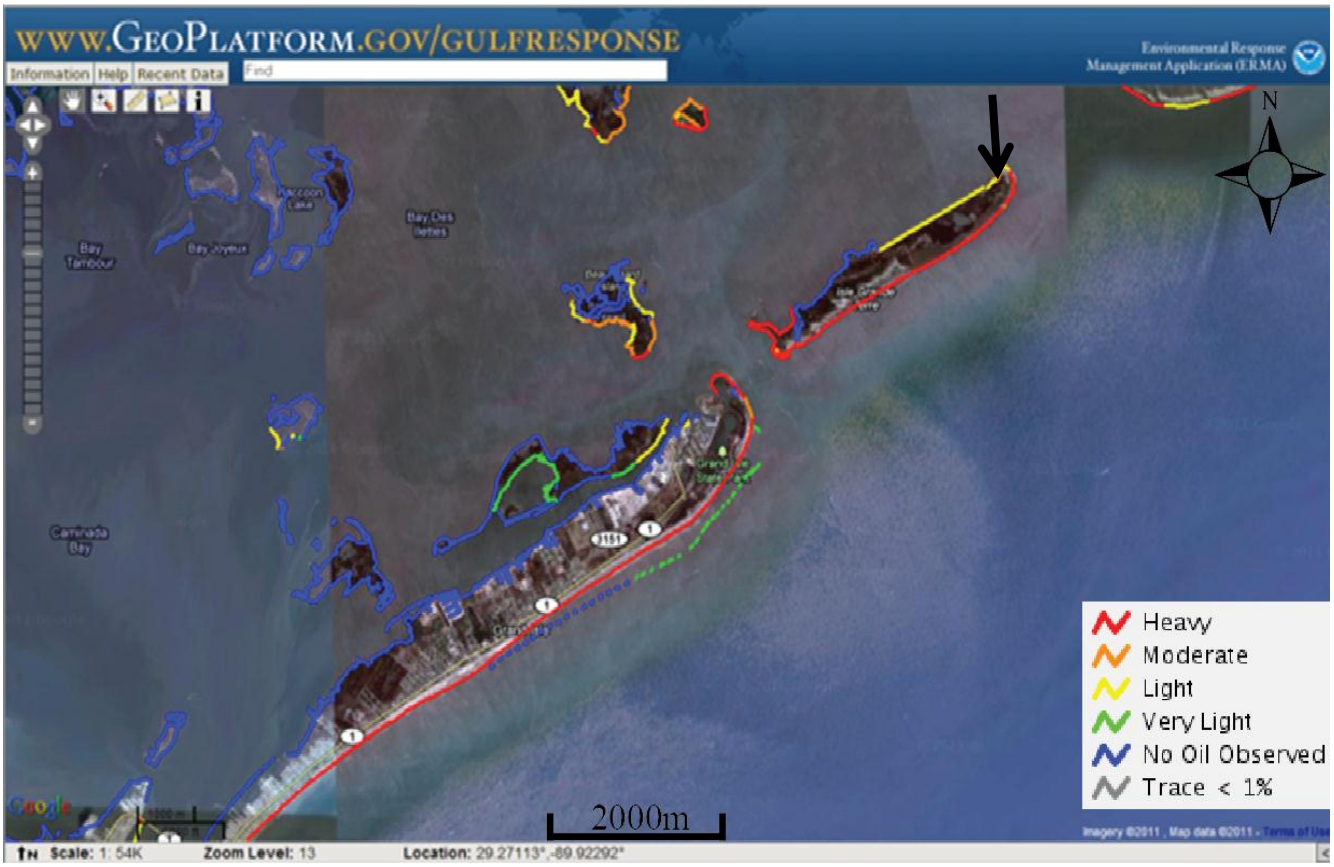

Figure 2. Map showing the concentration of contamination of crude oil due to the Deepwater Horizon oil spill. The black arrow is pointing towards the northeast corner of Grand Terra 1 where we chose to use as our site.

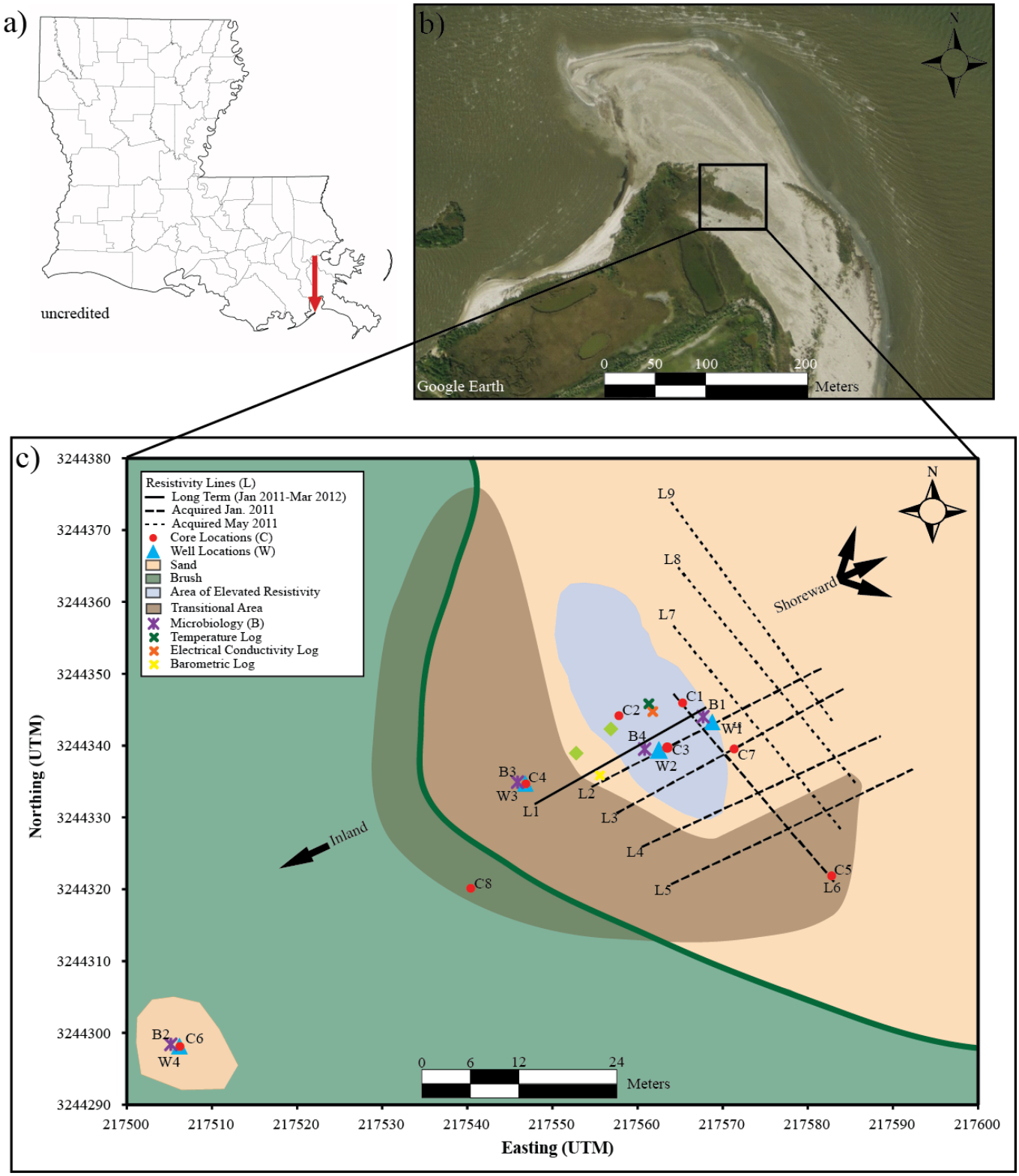

Figure 3. Location of the site starting with a) the state of Louisiana, followed by b) a satellite image of the northwestern tip of the island Grand Terra 1,while c) is the study map showing locations of instruments and sampling areas.

CHAPTER II

METHODOLOGY

2.1 Introduction

Electrical resistivity (ER) and electromagnetic (EM) methods are frequently applied to soil mapping and the detection of contaminated areas. The most common methods are based on the temporal and spatial observation of electrical parameters, including electrical resistivity in direct current, electrical permittivity, and magnetic susceptibility. Electrical techniques are sensitive to the petrophysical and hydrologic properties of soil (porosity, fluid content, salinity) and to the soil texture and structure (grain size, arrangement, and pore space) (Godio et al., 2010).

In the absence of clays, Archie's Law (1942), describes the bulk conductivity of consolidated sediments:

$$\sigma_e = a\phi^m S_w^n \sigma_w \qquad (1)$$

where σ_e is the bulk conductivity of the sediments, a is an empirical factor, ϕ is the fractional pore volume (porosity), m is a cementation factor, S_w is the fraction of the pores containing fluid, n is a saturation coefficient, and σ_w is the electrical conductivity of the pore fluid. Archie's Law suggest that three main components control the bulk conductivity of sediments; the petrophysical characteristic of the sediments (a, ϕ^m), fluid saturation (S_w^n), and the electrical properties of the fluid (σ_w).

2.2 Geophysics

2.2.1. Electrical Resistivity and Electromagnetic Surveys: Two surveys were conducted in connection with this research: the acquisition of eight ER lines to spatially detect and delineate the presence of crude oil and a companion study by Rutgers University using long-term ER survey to capture the biogeophysical signals resulting from the physical, chemical, and microbial transformation of crude oil in a highly saline environment. In total, nine 2-D ER lines were acquired over a span of fourteen months. A IRIS Syscal Pro was used to acquire ER data utilizing a dipole-dipole array. Line 1 was installed for the purpose of long term monitoring by a companion study by Rutgers University. This line was installed November 2010 and (besides a couple breaks due to technical issues) collected data twice a day until January of 2012. It was orientated SW-NE and cut a crossed the area of elevated resistivity. The array consisted of 46 stainless steel electrodes with a 0.5 m spacing. Data from lines 2 through 6 were acquired over a two-day period in mid-January 2011. Lines 2 through 5 were parallel to line 1 with a SW-NE orientation and were each separated by 10 m. Data from line 6 was acquired with a SE-NW orientation, perpendicular to lines 1 through 5. The array for lines 2 through 6 consisted of 63 stainless steel electrodes with a spacing of 0.5 m. Data from lines 7 through 9 were acquired May 19th 2011 and ran parallel to line 6 with a SE-NW orientation. The array for lines 7 through 9 consisted of 72 stainless steel electrodes with a spacing of .5m.

EM data was acquired on January 11th, 2011 using an AeroQuest GEM2. The GEM2 is a multi-frequency EM instrument equipped with a GPS. Data was collected over a large area that encompassed both the main study area as well as our background area using four frequencies: 1050, 5010, 20010, and 60030Hz.

2.2.2 Computer Processing: Apparent-resistivity data were inverted using AGI EarthImager, and a least-squares inversion technique was used for the inversion subroutine.

2.3 Geochemistry

2.3.1 Piezometer Installation: A piezometer network was installed at 4 different locations within the survey site. Piezometer locations 1, 2, and 3 are located along ER lines 1 and 2, while piezometer 4 is located in the background area. Multilevel piezometers (MPLs) were installed at each location for groundwater sampling. The MLPs were constructed of 1/8 inch inner diameter polyvinyl tubing fitted with a 10 cm screens. The piezometers were installed at intervals of 25 cm from the surface and reached a maximum depth of 200 cm.

2.3.2 Groundwater Sampling and Analysis: Water samples were collected at all piezometer clusters (MPLs) locations on May 19th and 20th 2011. Water temperature, specific conductance (SPC), dissolved oxygen (DO), oxidation-reduction potential (ORP), and pH were measure for each piezometer using a Yellow Springs Instrument (YSI) multi parameter probe calibrated according to the manufacturer's instructions. The YSI probe was immersed into a flow through cell into which water was pumped using a peristaltic pump. Readings were recorded after the pH, conductivity, and temperatures stabilized and before samples were collected for chemical and isotope analyses. Samples collected for chemical analyses were filtered through 0.45 µm syringe filters. Aliquots of the filtered water were stored in HDP bottles unacidified for anion analysis and acidified with nitric acid to pH < 2 for cations and metal analysis. Samples were transported on ice and stored at 4°C until analyses.). Immediately after filtration in the field, aliquots of the water were used to determine total alkalinity by acid titration (Hach Company, 1992) and ferrous iron (Fe^{2+}) by colorimetry using the Phenanthroline method (CHEMetrics Inc., 2004). Samples for DIC extraction and $\delta^{13}C_{DIC}$ measurements were filtered directly into pre-ecacu8ated vials loaded with 85% phosphoric acid and magnetic stir bars (Atekwana and Krishnamurthy. 1998.

Anions were analyzed by ion chromatography and cations and metals were analyzed by an inductively coupled plasma optical emission spectrometry (ICPOES). DIC was extracted from samples in the laboratory under vacuum and the concentration determined empirically from

measured CO_2 pressures (Atekwana and Krishnamurthy, 1998). The extracted CO_2 was stored in Pyrex tubes and later analyzed for $\delta^{13}C$ by isotope ratio mass spectrometry. The $\delta^{13}C$ is reported in the delta notation in per mill (‰) relative to Vienna Pee Dee Belemnite (VPDB) carbon standard with a precision of better than 0.1‰.

2.3.3 Barometric, Water Level, Temperature, and Electrical Conductivity: Barometric, water level, and temperature data was collected every 25 minutes from 1/11/2011 till 8/15/2011. An electrical conductivity logger was placed at a depth of 0.25 m bgs and collected data twice a day (at 8:00 am and 8:00 pm) from 8/15/2011 through 1/11/2012.

2.4 Soil Sampling and Analysis

2.4.1 Sediment Core Extraction and Preparation: Sixteen soil cores were collected from eight locations at the site. One core was collected in November 2010 in the depressed area. Five cores were collected in January 2011; three (1A, 1B, and 1C) from the area of elevated resistivity, one (6E) from the transitional, and one (8A) from the background area. Ten cores were collected in May 2011; three (2A, 2B, 3A) from the area of elevated resistivity, three (4A, 5A, 7A) from the transitional area, and four (6A, 6B, 6C, 6D) from background. Cores were collected by manually driving 1 m long, 1½ inch diameter clear polycarbonate tubing into the ground. After extraction they were cut, capped, sealed, and placed on ice for transport. Once at Oklahoma State University they were transferred into a large freezer for storage. Six cores (1A, 2A, 3A, 4A, 5A, and 6A) were chosen based on there location within area of elevated resistivity, the transitional, and the background area, as well as proximity to resistivity lines and piezometers locations. Soil samples from these cores were extracted in 2 cm intervals, were dried, and ground by hand using an agate mortar and pestle. These samples were used for grain size analysis, magnetic susceptibility. Total organic and inorganic carbon analysis, and x-ray fluorescence.

2.4.2 Grain Size Analysis: Sediment grain-size distribution was determined for Cores 1A, 3A, 4A, and 5A to better understand distribution throughout the impacted and transitional areas. The percent of medium (0.5-0.25 mm), fine grain (0.25-0.125 mm), and very-fine grained (0.125-0.062 mm) sand were determined by sieve analysis after drying the sediments to a constant weight and sieving using screens NO. 60, 100, 120, and 140. Sediment samples used for sieving were extracted using a 2 cm or 4 cm interval.

2.4.3 Microbiology: Soil and sediment samples were collected in sterile plastic containers at various locations and at different depths above the water table at the site. Three of the samples locations (B1, B3, and B4) were located in the depressed area of the site and one (B2) in the background area. Samples were analyzed for microbial diversity and for hydrocarbon degrading potential by Dr. Babu Fathpure at Oklahoma State University Department of microbiology and molecular genetics

2.4.4 Magnetic Susceptibility: Variable concentrations of magnetizeable materials such as ferromagnetic, paramagnetic, and diamagnetic minerals present in sediments affect the strength of magnetism in a given sample (Ellwood et al., 2004). Magnetic susceptibility (MS) is a technique used to determine the concentration of magnetizeable materials in a sample. Low frequency magnetic susceptibility (X_{lf}) was measured for each sample collected from the six cores from the site using a Bartington MS2 magnetic susceptibility meter with an MS2B dual frequency sensor.

2.4.5 Total Organic and Inorganic Carbon: Total inorganic carbon (TIC) and total organic carbon (TOC) concentrations were determined using a CM5014 coulometer equipped with a CM5130 Acidification Module and CM5300 Furnace Module. For TIC analysis, a pre-weighed sample was reacted with 2N $HClO_4$ to release CO_2, which was titrated electronically. Total carbon (TC) was determined by combusting a pre-weighed sample in the furnace module at 950°C. TOC was determined by calculated the difference between the TC and TIC values. Pure

calcite was analyzed each day to ensure instrument stability. Calcite concentrations were measured within 95%. Measured concentrations of the calcite standards were used to correct measured sample concentrations for any instrumental inaccuracies.

2.4.6 X-Ray Fluorescence (XRF): Iron (Fe), Manganese (Mn), and Sulfur (S) concentrations were measured using the handheld Thremo Scientific Niton XL3t x-ray fluorescence analyzer. The standard (USGS SCo-1) was used to correct each measured concentration for any errors associated with matrix effects in the XRF. The measured concentrations from the standard were compared to the certified values. The differences between measured and certified values were used to calculate correction factors which were then applied to all analyses for a given day.

2.5 Control Experiments

2.5.1 Column Setup: Two in laboratory experiments were conducted using columns to gain insights into how variations in the percent of oil saturation and salinity concentration govern the electrical properties at our site. The measurement columns for both experiments were constructed of polyvinyl chloride pipe (PVC), column height was 5 cm with an interior diameter of 3.3 cm. Two coiled silver-silver chloride (Ag-AgCl) current electrodes were placed at the end of each column. The coil technique allows for a greater current distribution throughout the sample. Two Ag-AgCl potential electrodes were placed equidistant along the long axis in a Wenner array, with an a-spacing of 2 cm between each electrode. All Columns were packed with sand (U.S. Silica, Ottawa Standard, 20 – 30 (850 – 520 μm) mesh), "clean" sands were used for the column measurements due to the inability of sacrificing cores from the location at the time when these measurements were performed.

2.5.2 Variations in Salinity: To measure the variations in electrical response due to salinity, a mixture of DI water and varying amounts of NaCl were used to create a "salinity range" spanning

20-34 mg/l, one of these salinity solutions was then mixed with the sand grains. Once the grains were coated, they were packed and sealed into a column and flushed with the salinity solution until the column was completely saturated, followed by a measurement.

2.5.3 Oil Saturation: To measure how the electrical resistivity would change with variations in the percent oil saturation columns were created. First an average salinity of 30.5 mg/l was determined by averaging the salinities seen at W#1. A total volume of 30.00 ml was used when determining the different rations of crude oil to salt water which would produce the percent of crude oil to be added. The salt water was first added to clean sand grains in order to establish that the "salt water" was in the wetting phase, this was followed by the addition of the crude oil. This was thoroughly mixed and placed in a column for measurements.

CHAPTER III

RESULTS

3.1 Geophysical

3.1.1 Geophysical Results: The resistivity inversion results of selected profiles (L2, L3, L5, L6, L9) are presented in Figures 4 and the rest of the profiles (L4, L7, and L8) are located in the appendix. Three distinct layers can be observed throughout the majority of the 2D resistivity lines shown in Figure 4. Layer 1 is occurs between 0.0 to 0.5m bgs with a resistivity ranging from 0.65 Ωm – 1.2 Ωm; 2) layer 2 is found between depths of 0.25 m and 1.20 m bgs with resistivity ranging from 1.5 Ωm -2.3 Ωm, layer 3 extends to the base of the 2D apparent resistivity section with resistivity values < 1 Ωm Regardless of the depth of layer 2), a transition of decreasing resistivity with depth is always present. The 2nd layer of resistivity can be seen though out all of L2 (Figure 4a) at a depth of 0.20m to 1.10m. A similar structure is seen in L3 (Figure 4b) with the only real difference being the magnitude of the anomalous resistivity response which appears to be slightly attenuated compared to that of L2. The response of the 2nd layer in L5 is found in the first and last 6 m of the line, while the middle 25m appears to have a uniformly low apparent resistivity response of 0.65 Ωm at all depths (Figure. 4c).

Line 6 shows the 2nd layer, centered at a depth of 0.8 m and increasing in magnitude to the NW from 0.89Ωm at the beginning of the line (southeast end) to 2.3 Ωm near the end of the line to the NW, the anomalous electrical resistivity increase becomes more pronounced at the 20 m mark (right before L6 intersects L3) of L6 (Figure 4d).

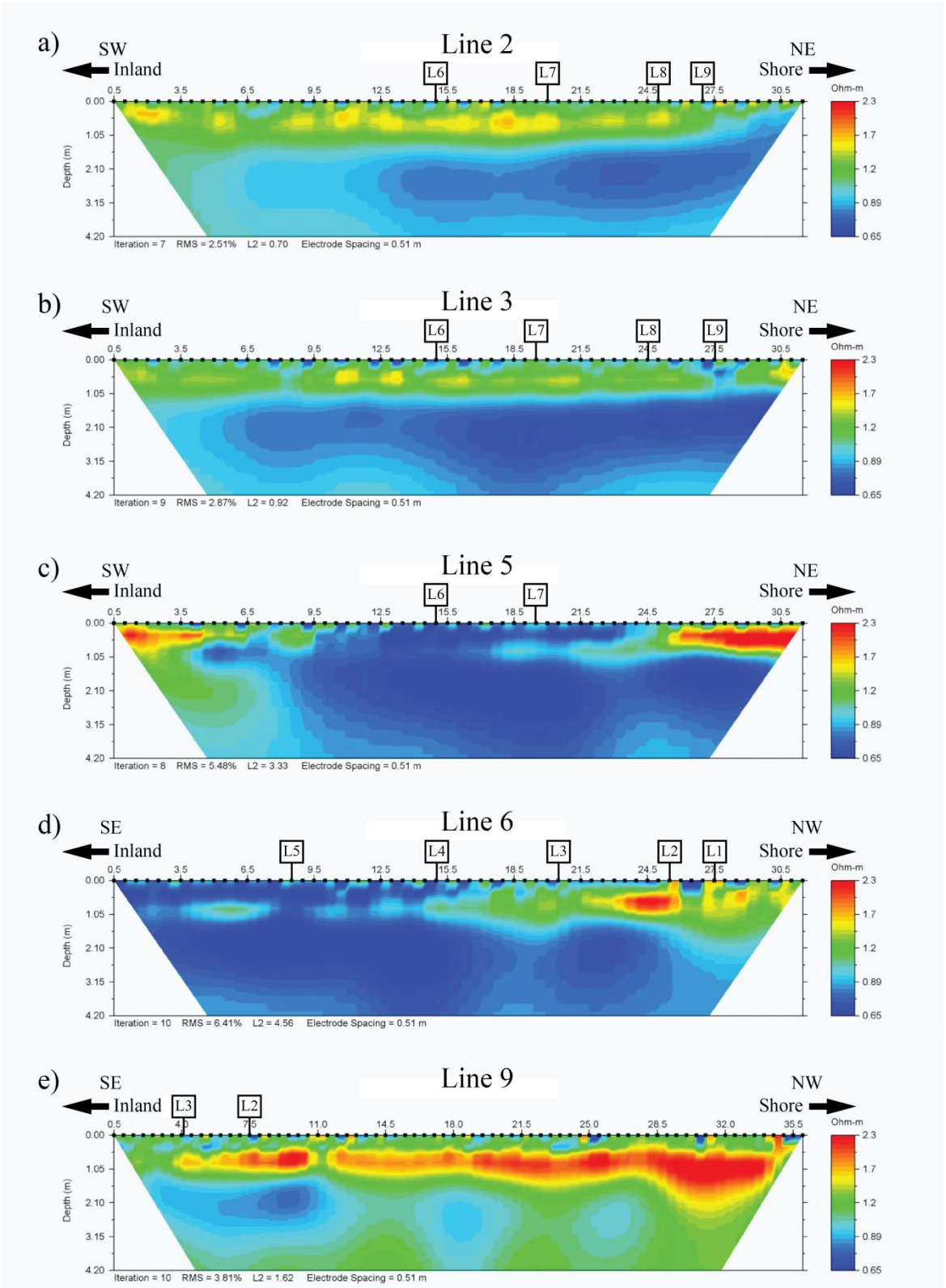

Figure 4. 2D electrical resistivity (ER) images of a) L2, b) L3, c) L5, d) L6, and e) L9

Apparent resistivity depth slices (Figure 5) were created by exporting each processed ER line in a XYZ format and contouring the apparent resistivity data at the depths of 0.5 m, 1.0 m, 1.5m, and 2.0 m (Figure 5 a, b, c, and d, respectively). The layer of relatively higher resistivity between the depth of 0.25 m and 1.20 m is seen in the 2D ER lines (Figure 4) while the depth slices (Figure 5) help illustrate the increase in apparent resistivity as you progress from SE to NW.

The contour images of EM data shown in Figure 6 show an increase in conductivity with depth through the site. There is an area of consistently higher conductivity, regardless of the depth within the area of elevated resistivity. It is spatially the largest in the lowest measured frequency of 1050 Hz (Figure 6a) and appears to be centered approximately where L5 and L6 intersect, just to the SE of the area of elevated resistivity. As the measured frequency increases (the skin depth decreases) this conductivity anomaly gradually pinches out as it approaches the surface (Figure 6d).The conductivity within the area of elevated resistivity of Figure 6 decreases starting at a range of 750 to 1050mS/m at a skin depth of 2.67m (Figure 6a) to a range of 450 to 750mS/m at a skin depth of 0.97m (Figure 6d). This shows as the depth decreases, the conductivity of the entire site decrease with the lowest recorded conductivity observed towards the NW.

3.2 Geochemistry

3.2.1 Physical, Chemical, and Isotopic Properties of Groundwater: The salinity measured at the site ranged from 14.07 to 80.98 mg/l in the ground water, with the highest values recorded at the background location (Table 1; Figure 7). Piezometers inside the area of elevated resistivity show a similar trends; the highest value recorded in piezometer cluster 1 and 2 occur at a depth of 25 cm of 31.5 and 33.8 mg/l respectively, with a lower value within each piezometer cluster at a depth of 50 cm of 24.9 mg/l for well 1 and 30.0 mg/l. This is followed by a slow increase in salinity with depth for both piezometer clusters 1 and 2 (Table 1; Figure 7).

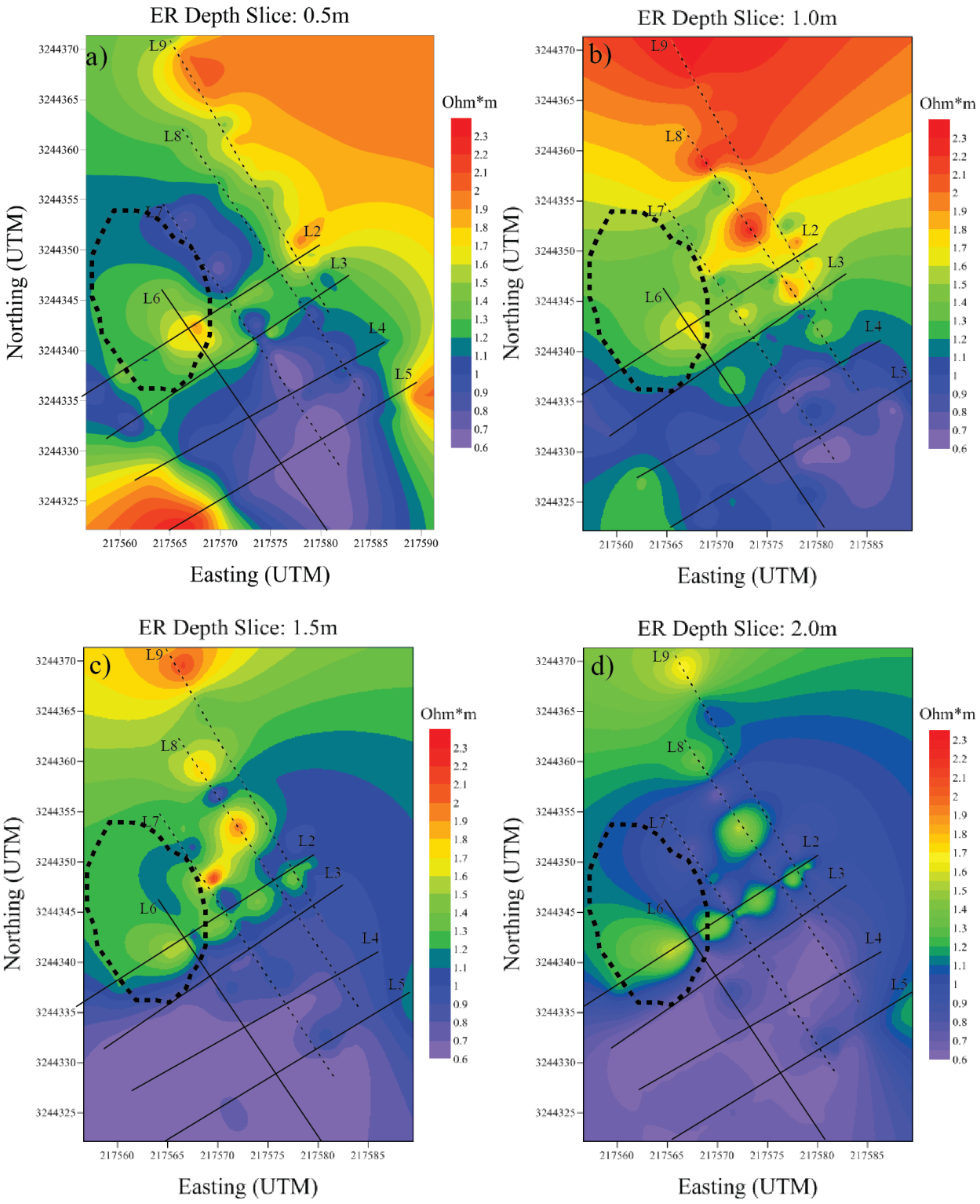

Figure 5. Depth slices created from contouring of data extracted from electrical resistivity lines. L1 to L9 represent the locations of electrical resistivity profiles shown in Figure 4. The area within the dotted line represents the area of elevated resistivity.

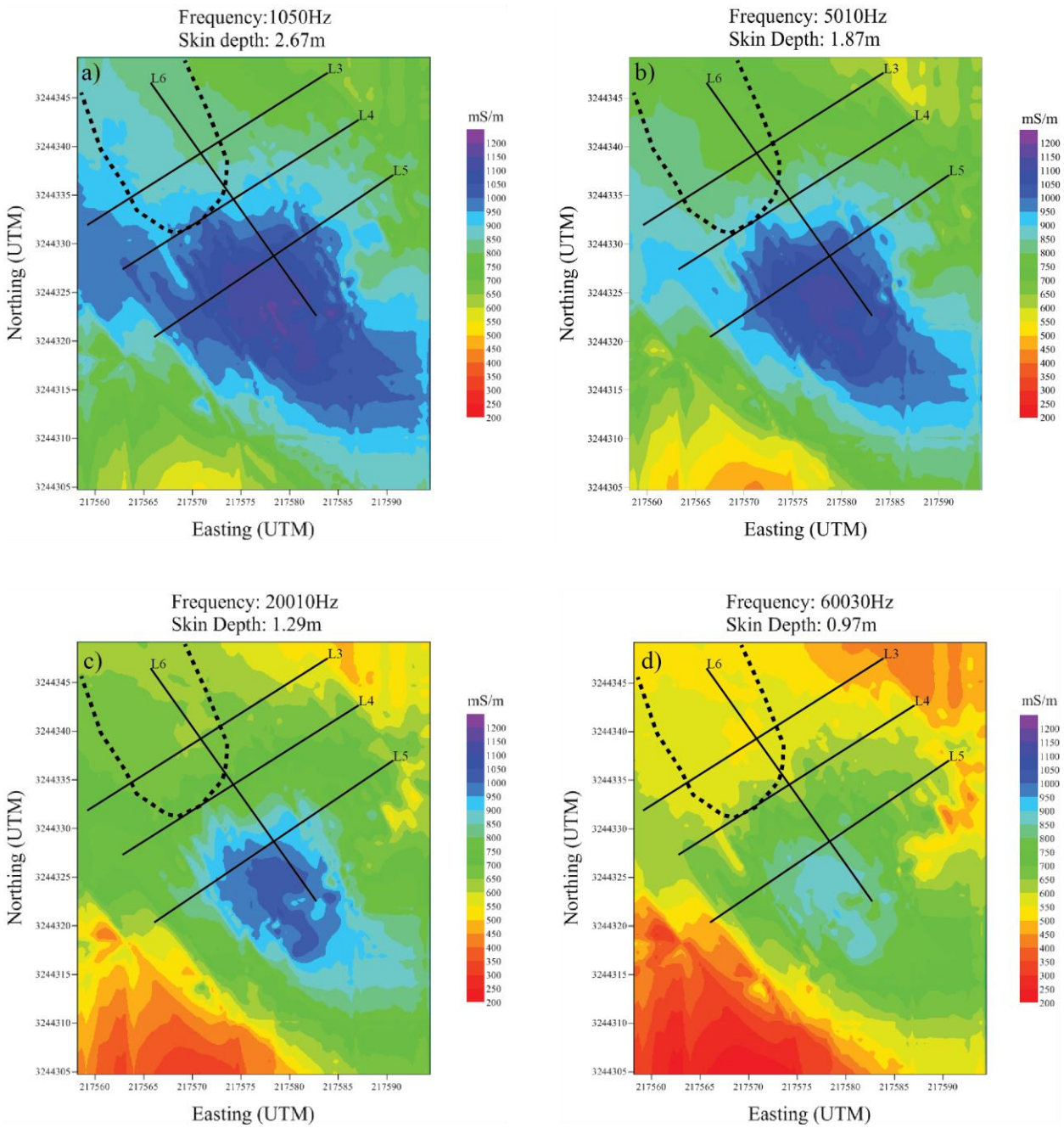

Figure 6. Bulk electrical conductivity data at different frequencies obtained from the GEM2 system and the calculated depths with lines representing the location of electrical resistivity line. a) bulk electrical conductivity at 1050 Hz, skin depth of 2.67 m b) 5010 Hz, skin depth of 1.87 m c) 20010 Hz, skin depth of 1.29 m and d) 60030 Hz, skin depth of 0.97m. The dashed line represents the extent of the area of elevated resistivity.

Table 1.D is the sample depth (cm bgs), temperature (degree C), and pH. Total dissolved solids (TDS), salinity are both represented in mg/l, and specific conductance (SPC) is represented in mS/m. Alkalinity, CL, SO_4^{-2}, NO_3^-, Na, K, Ca, Fe^{+3}, and Mg are all represented in mg/l. Dissolved oxygen (DO) is in %, dissolved inorganic content (DIC) is represented in $mgCO_2/l$, and isotope ratio of dissolved inorganic carbon ($\delta^{13}C$) seen in ‰.

D	T	pH	TDS	Salinity	SPC	Alkalinity	Cl	SO_4^{-2}	NO_2^-	Na	K	Ca	Fe	Mn	DO	DIC	$\delta^{13}C_{DIC}$
WELL LOCATION #1																	
0	33.69	8.54	21.41	15.82	32.94	109	10466.13	1583.518	11.3447	6113.5	235.5	277	0.3	6.635968	227	78.68988	-12.189
10	25.83	7.06	29.23	25.99	44.85	242	16125.54	2301.694	3.6581	9093.2	341.7	391.7	0.3	35.55956	48.8	203.7839	-12.311
25	24.68	6.94	33.36	31.45	51.31	308	17852.18	2429.469	3.8625	10352.2	398.9	409	7.1	147.6402	10.3	295.9584	-13.807
50	24.41	7.22	28.39	24.91	43.57	371	15543.53	1919.363	12.0668	8545.3	317.9	302.7	10.9	259.2965	49.7	369.5784	-12.61
75	24.42	7.19	29.21	25.96	44.82	390	15821.28	1869.136	19.0293	8877	304.4	351.7	17.8	157.6659	60.09	382.1476	-12.567
100	24.03	7.33	30.55	27.8	47	375	16462.84	2020.965	14.6540	9554	312.9	363.8	13.1	93.96305	3	374.6659	-12.146
125	23.96	7.06	30.43	27.72	46.9	358	17634.78	2102.668	12.6482	10697.7	360.3	434.5	9.8	56.76637	64.6	404.5927	-12.436
150	23.94	7.31	32.29	30.1	49.72	427	16774.1	1981.448	5.9148	9767	326.1	396	9.7	118.7604	79.9	395.0162	-12.3
WELL LOCATION #2																	
10	31.92	6.92	27.65	24.05	42.56	175	13939.74	2149.34	10.9467	7518.4	296.5	350.4	3.9	46.33128	49.5	165.5656	-9.802
25	26.74	7.16	32.11	33.82	54.12	339	17927.36	2566.862	14.2484	9665.3	377.9	477.3	15.2	204.0238	48.9	321.8891	-11.436
50	24.33	7.17	32.23	29.99	49.59	394	17888.99	2219.05	19.7957	9903.7	322.2	440.8	13.5	328.038	24.8	384.9819	-11.462
75	24.43	7.22	33	30.99	50.77	512	17893.47	2157.721	4.1995	10183.8	327.7	432.3	16.6	319.9364	1.9	488.3526	-11.75
100	24.28	7.27	33.69	31.84	51.77	496	18152.62	2215.608	14.8513	10432.1	334.1	445.4	16.1	235.7314	3.1	480.1843	-11.75
125	24.28	7.13	33.8	32.01	51.98	584	18660.48	2199.51	4.6990	10225.9	333.4	414.9	23.6	285.9218	61.6	572.2884	-11.809
150	23.87	7.13	24.9	33.46	53.69	734	19154.96	2245.429	13.7255	10717.6	348.2	422.9	24.8	342.5554	3.2	725.232	-11.9
WELL LOCATION #3																	
50	26.32	7.22	19.98	14.07	30.75	2286	9297.316	151.1639	6.8902	5901.6	230.6	88.7	3	99.84248	58.6	2340.188	-9.336
75	25.57	7.17	25.04	20.64	38.52	2152	12921.31	227.5726	14.3285	7131.2	281.1	157.0	15	226.2027	7	2268.363	-9.699
100	24.59	6.96	33.24	31.31	51.15	1819	18639.78	1084.325	3.6898	9926.3	335.4	421.4	35	79.83319	13.8	1868.841	-11.005
125	24.4	6.85	36.91	36.08	56.79	1204	21074.65	1645.385	19.5080	10664.7	329.8	471.5	43	167.8998	61.1	1376.545	-11.358
150	23.69	6.95	38.55	38.21	59.31	1040	21832.9	2201.055	13.7635	11944.5	365.9	495.5	63	189.8378	6.6	1277.786	-11.154
WELL LOCATION #4																	
25	28.36	6.73	68.8	80.98	109.9	1182	43497.62	3952.276	4.5479	26255.3	865.6	412.1	6.3	55.78728	46.8	1217.933	-8.66
50	28.82	6.87	52.69	56.61	81.07	2176	31361.46	1357.972	4.4116	17875.3	542.9	318.9	4.3	52.69442	14.2	2389.655	-13.195
75	26.4	6.62	50.38	53.59	77.5	2024	29861.43	2057.091	6.7630	16957.4	496.1	373.5	58.4	95.21581	9	2174.182	-15.53
100	25.83	6.73	53.38	57.49	82.11	1814	32424.78	3001.155	8.6047	18243.1	542.1	425.7	61.8	67.06641	5.7	1888.293	-16.143
125	25.49	6.77	55.79	60.63	85.82	1300	36516.34	4860.357	2.7223	21400.4	675	583.6	65	20.6884	49.2	730.654	-12.689
150	25.06	6.88	58.61	64.29	90.17	824	32923.07	3676.593	4.0520	18989.7	579.5	498.7	35	50.83867	2.8	1387.019	-15.681
175	225.61	7.04	60.03	66.14	92.33	671	35255.13	4566.816	3.1271	19907.8	613.2	564.4	23	28.56127	67.9	854.3221	-13.993
200	24.45	7.2	61.61	68.2	94.78	664	36772.55	4886.502	7.1052	21693	664.2	573.6	20.1	23.8567	1.6	701.0793	-12.941

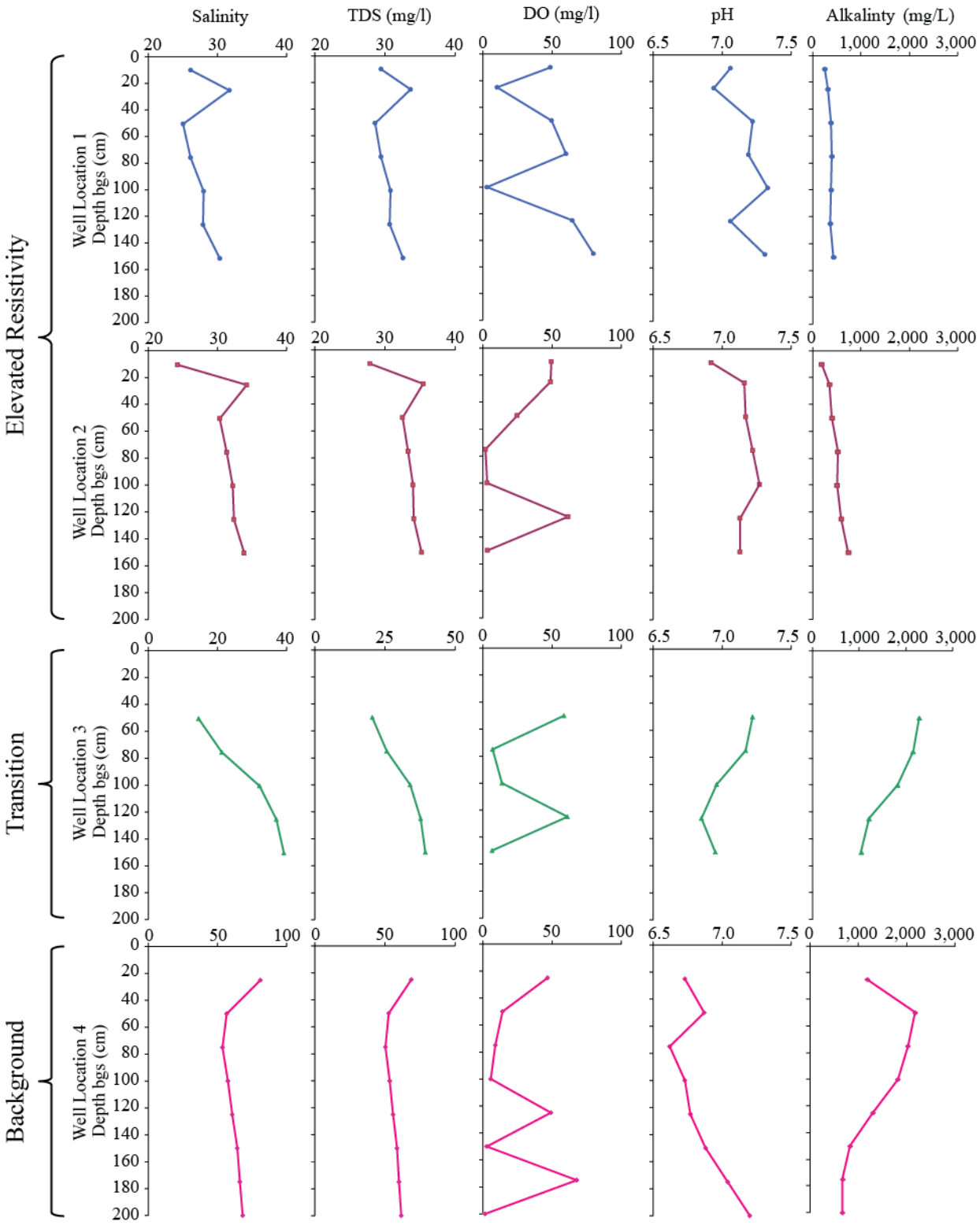

Figure 7. Vertical profiles of Salinity, total dissolved solids (TDS), dissolved oxygen (DO) pH, and alkalinity in the groundwater for locations in the area of elevated resistivity (W#1/W#2), for the transition area (W#3), and for the background area (W#4).

The total dissolved solids (TDS) show an identical trend observed in salinity (Table 1; Figure 7). Piezometer cluster 1 shows two distinct decreases in the dissolved oxygen (DO) values approaching 0mg/L at depths 25 cm and 100 cm while the rest of the values were between 50 to 80 %saturation (Table 1; Figure 7). The DO values of piezometer cluster 2, 3, and 4 show similar trends, with values greater than 25 %saturation above 50 cm bgs while lows (less than 8 %saturation) from a depth of 75 cm to 150 cm with a spike of 61 %saturation at 125cm bgs(Table 1; Figure 7). Piezometer clusters 1 and 2 inside the area of elevated resistivity have the highest pH which ranged from 6.92-7.33. Standing water at the site had a pH value of 8.54 and piezometer cluster 4 had the lowest range of all wells of 6.62-7.2 and displayed a general trend of increasing pH with depth(Table 1; Figure 7). The groundwater samples within the impacted zone were lower in alkalinity than those of the transition and background (Table 1; Figure 7). Fe(II) values for the area of elevated resistivity were greater than the transitional and background between 25 cm to 50 cm bgs, at which the trend is reversed with both wells 3 and 4 showing values much greater than those piezometer clusters 1 and 2 (Table 1; Figure 8). Groundwater at piezometer cluster 1 and 2 show increases in dissolved inorganic carbon between depths of 50 cm to 120 cm of 204 to 375 mg CO_2/l and 321 to 480 mg CO_2/l respectively, while the background location were between 730 to 2340 mg CO_2/l (Table 1; Figure 8). Concentrations of Mn in groundwater at piezometer clusters 1 and 2 are highest at a depth of 50cm and were elevated with respect to groundwater at piezometer clusters 3 and 4 (Figure 8). Sulfate values for groundwater piezometer clusters in the area of elevated resistivity were lower between 50 cm to 125 cm bgs with their lowest value at a depth of 75 cm (Table 1). Ions Mg, Na, K, and Cl all show similar depth variations of the area of elevated resistivity and transitional area and are substantially lower in the concentration compared to the background (Table 1)

3.2.2 Hydrocarbon Analysis: All soil and groundwater samples sent out for analysis to both laboratories came back below practical quantitative limit (BPQL) for TPH (Tables 2, 3, and 4).

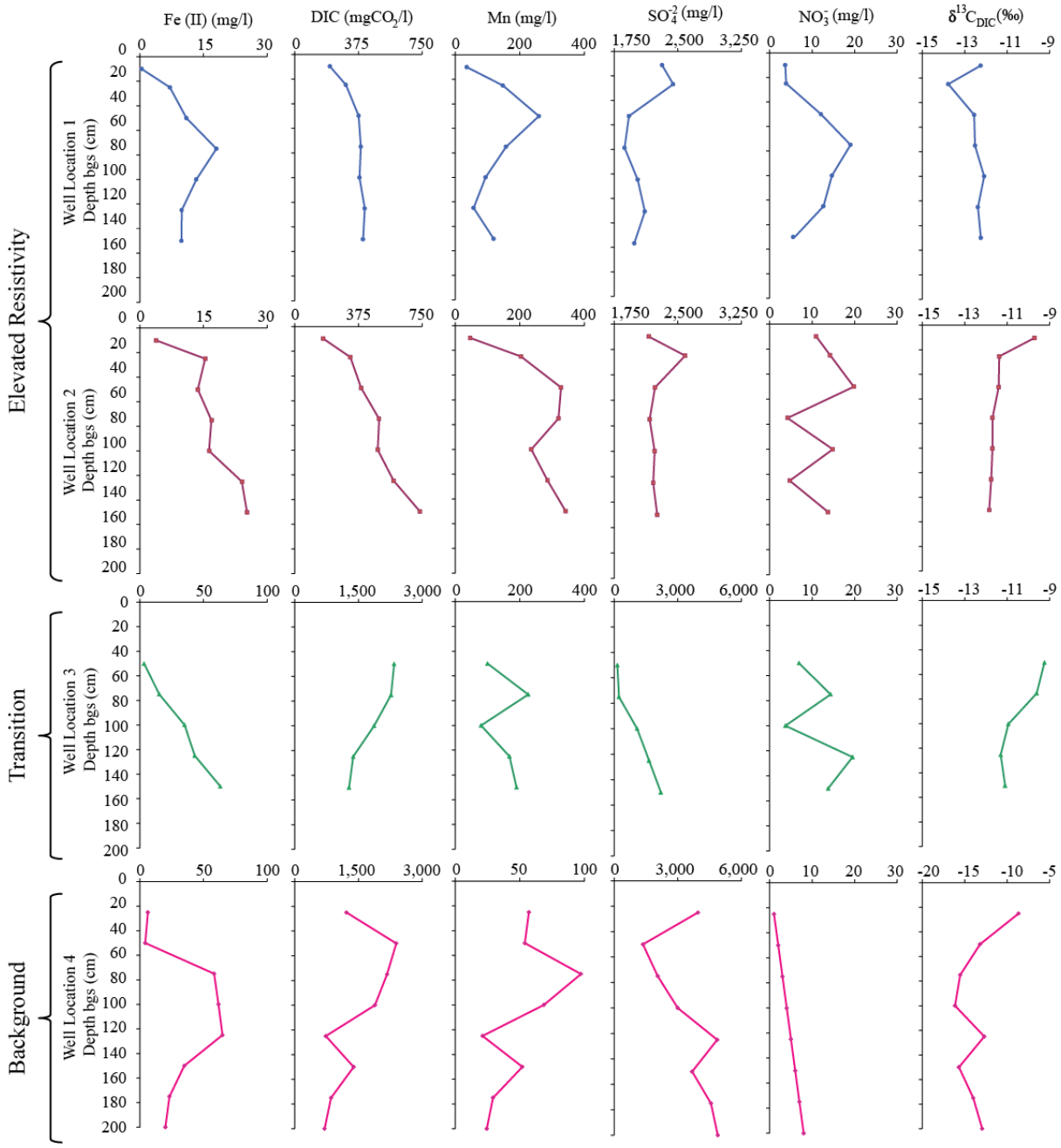

Figure 8. Vertical profiles of Fe(II)), dissolved inorganic carbon (DIC), Mn(II), SO_4^{-2}, and NO_3^-, and isotopic ratio of dissolved inorganic carbon ($\delta^{13}C_{DIC}$) in the groundwater for locations in the area of elevated resistivity (W#1/W#2), for the transition area (W#3), and for the background area (W#4).

Table 2. Results of soil samples collected on 11/17/2010 and 01/12/2011 from various areas within the elevated resistivity area, transitional, and background areas.

Sample	Date Collected	Type	Well Location	Collection Depth (cm)	C6 - C12	>C12 - C28	>C28 - C35	Total Petroleum Hydrocarbons	PQL#
S/2-14	11/17/2010	Soil	4	14	BPQL	BPQL	BPQL	BPQL	50
S/2-26	11/17/2010	Soil	4	26	BPQL	BPQL	BPQL	BPQL	46.3
S/3-20	11/17/2010	Soil	2	20	BPQL	BPQL	BPQL	BPQL	50
S/3-00	11/17/2010	Soil	2	0	BPQL	BPQL	BPQL	BPQL	46.7
S#1-12	1/12/2011	Soil	1	30.48	BPQL	BPQL	BPQL	BPQL	50
S#1-3	1/12/2011	Soil	1	7.62	BPQL	BPQL	BPQL	BPQL	50
S#2-8	1/12/2011	Soil	2	20.32	BPQL	BPQL	BPQL	BPQL	50
S#2-3	1/12/2011	Soil	2	7.62	BPQL	BPQL	BPQL	BPQL	50

Table 3. Results of water samples taken on 1/11/201 from various depths using the piezometers at well location 1 within the area of elevated resistivity, as well as a sample from the background area.

Sample	Date Collected	Type	Well Location	Collection Depth (cm)	C6 - C12	>C12 - C28	>C28 - C35	Total Petroleum Hydrocarbons	PQL#
W1-25	1/11/2011	Water	1	25	BPQL	BPQL	BPQL	BPQL	4.55
W1-50	1/11/2011	Water	1	50	BPQL	BPQL	BPQL	BPQL	4.55
W1-75	1/11/2011	Water	1	75	BPQL	BPQL	BPQL	BPQL	4.55
W1-1.0	1/11/2011	Water	1	100	BPQL	BPQL	BPQL	BPQL	4.55
W1-1.25	1/11/2011	Water	1	125	BPQL	BPQL	BPQL	BPQL	4.55
W1-1.5	1/11/2011	Water	1	150	BPQL	BPQL	BPQL	BPQL	4.55
W4-25	1/11/2011	Water	4	25	BPQL	BPQL	BPQL	BPQL	4.55

Table 4. Results of soil samples taken on 8/15/2011 from areas within the area of elevated resistivity (well locations 1 and 2) as well as samples from the background area.

Sample	Date Collected	Type	Well Location	Collection Depth (cm)	C6 - C12	>C12 - C28	>C28 - C35	Total Petroleum Hydrocarbons	PQL#
1.00	8/15/2011	Soil	1	0	BPQL	BPQL	BPQL	BPQL	50
1.05	8/15/2011	Soil	1	5	BPQL	BPQL	BPQL	BPQL	50
1.10	8/15/2011	Soil	1	10	BPQL	BPQL	BPQL	BPQL	50
1.15	8/15/2011	Soil	1	15	BPQL	BPQL	BPQL	BPQL	50
1.20	8/15/2011	Soil	1	20	BPQL	BPQL	BPQL	BPQL	50
2.00	8/15/2011	Soil	2	0	BPQL	BPQL	BPQL	BPQL	50
2.05	8/15/2011	Soil	2	5	BPQL	BPQL	BPQL	BPQL	50
2.10	8/15/2011	Soil	2	10	BPQL	BPQL	BPQL	BPQL	50
2.13	8/15/2011	Soil	2	13	BPQL	BPQL	BPQL	BPQL	50
2.15	8/15/2011	Soil	2	15	BPQL	BPQL	BPQL	BPQL	50
2.20	8/15/2011	Soil	2	20	BPQL	BPQL	BPQL	BPQL	50
3.00	8/15/2011	Soil	4	0	BPQL	BPQL	BPQL	BPQL	50
3.05	8/15/2011	Soil	4	5	BPQL	BPQL	BPQL	BPQL	50
3.10	8/15/2011	Soil	4	10	BPQL	BPQL	BPQL	BPQL	50
3.15	8/15/2011	Soil	4	15	BPQL	BPQL	BPQL	BPQL	50
3.20	8/15/2011	Soil	4	20	BPQL	BPQL	BPQL	BPQL	50

3.2.3 Electrical Conductivity: The electrical conductivity logger data in Figure 9 shows two distinct areas of measured EC separated by a sharp decrease. The first is from 08/15/2011 to 11/10/2011, where the average measured EC is 2002 mS/m. The second spans from 11/30/2011 to 1/11/2012 where the average EC is 1075 mS/m. The data between 11/11/2011 and 11/29/2011 shows an average decrease in conductivity of approximately 85 mS/m per day (Figure 9).

3.3 Soil Sampling and Analysis

3.3.1 Grain size Distribution: All cores tested were predominately composed (>69%) of fine grain sand (Figure 10). Core 1A had a higher percent of very fine grain sand ranging from 10%-26% throughout the core, while cores 4A and 3A ranged from 1%-6% (Figure 10c) and 4%-10%Figure 10b) respectively. Based on visual analysis during the sieving, any medium grain size peak in all sampled cores was the result of high amount of shell fragments.

3.3.2 Magnetic Susceptibility: Cores 1A, 2A, and 3A located in the area of elevated resistivity. Core 1A has two peaks at 66 cm and 72 cm of 31 (10^{-5} SI/cm^3/g) and 30 (10^{-5}SI/cm^3/g), from 70 cm through the end of the core at 90 cm the average reading is 23 (10^{-5}SI/cm^3/g) (Figure 11a). Core 2A displays a large sharp peak of 77 (10^{-5} SI/cm^3/g) at a depth of 4 cm followed by a nearly constant value of 10 (10^{-5} SI/cm^3/g) to a depth of 50 cm where a strong peak of 39 (10^{-5}SI/cm^3/g) is centered at a depth of 58 cm, this is followed by an elevated average reading of approximately 22 (10^{-5} SI/cm^3/g) starting at 64 cm till the end of the core at 96 cm (Figure 11b). Core 3A has two noticeable spikes at 62 cm and 76 cm registering 42 (10^{-5} SI/cm^3/g) and 38 (10^{-5}SI/cm^3/g) respectively (Figure 11c). Cores 4A and 5A are located in the transitional area of the site. Core 4A displays peaks at depths of 6 cm, 64 cm, and 76 cm, of 46 (10^{-5} SI/cm^3/g), 46 (10^{-5}SI/cm^3/g), and 42 (10^{-5} SI/cm^3/g) respectively (Figure 11d). The area

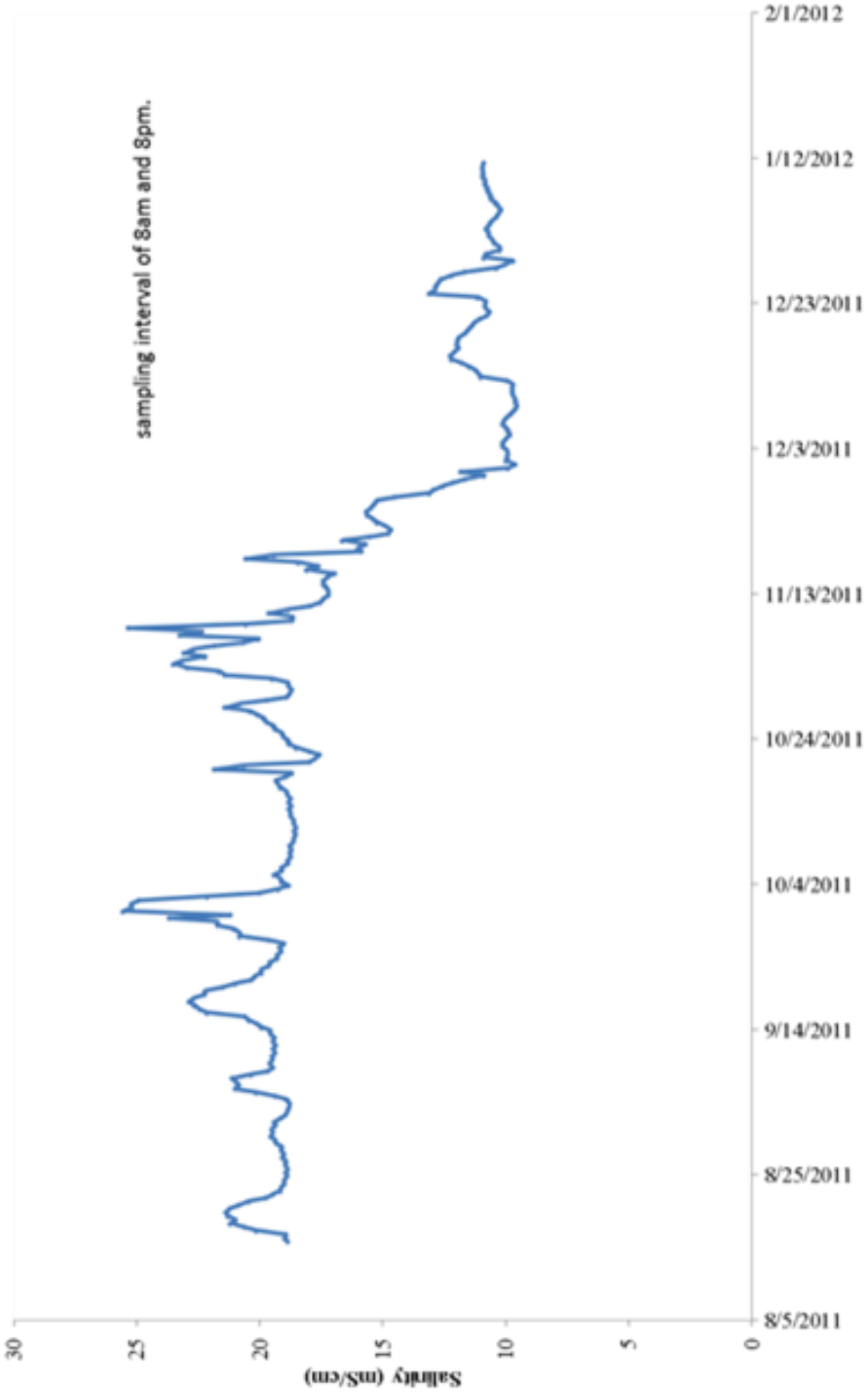

Figure 9. Temporal variations in monthly recorded maximum sea level data (National Oceanic and Atmospheric Administration) and the conductivity data collected by the logger on site.

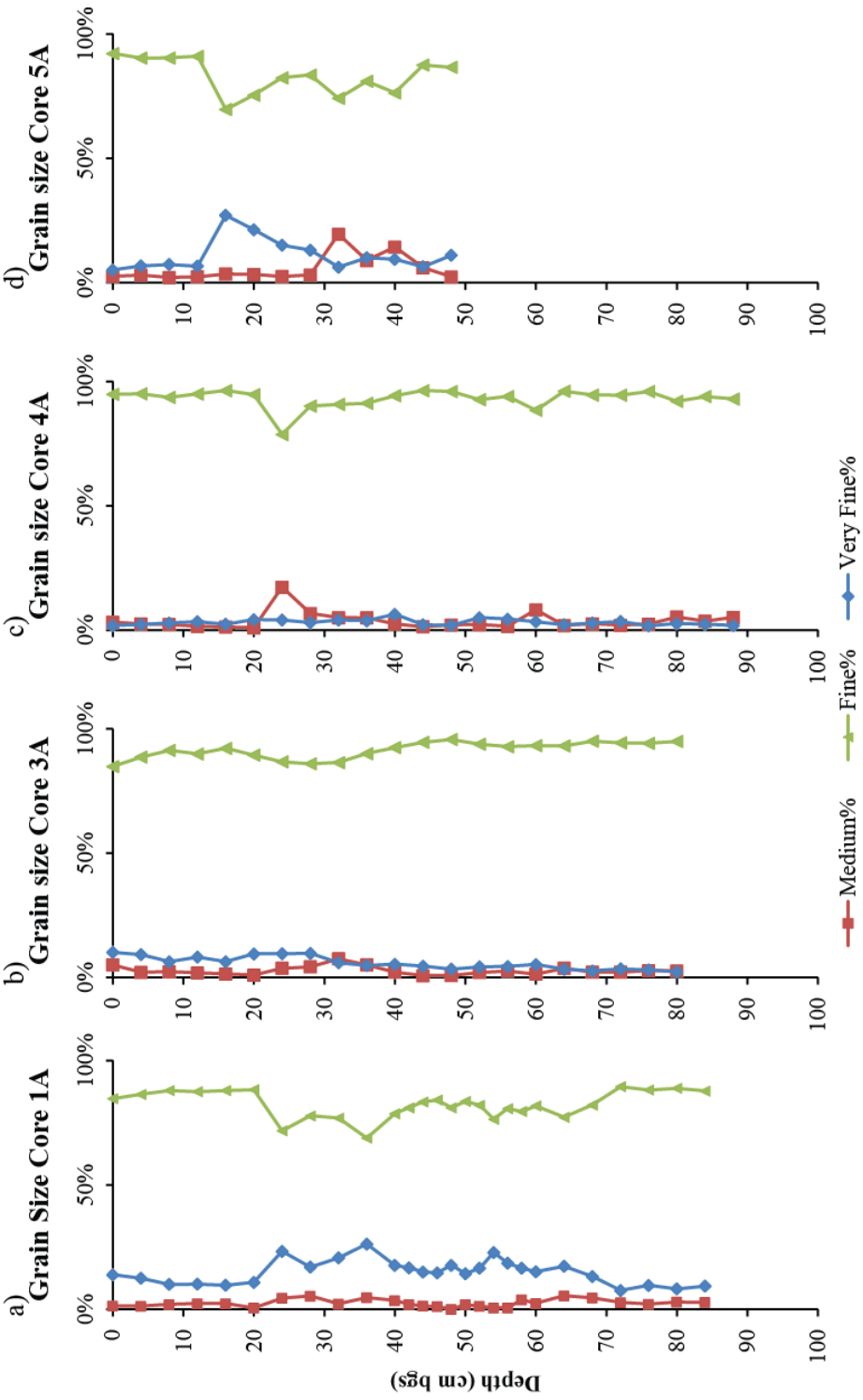

Figure 10. Grain size distribution for samples from of cores a)1A, b) 3A, c) 4A, and d)5A represented by percent composition by grain size

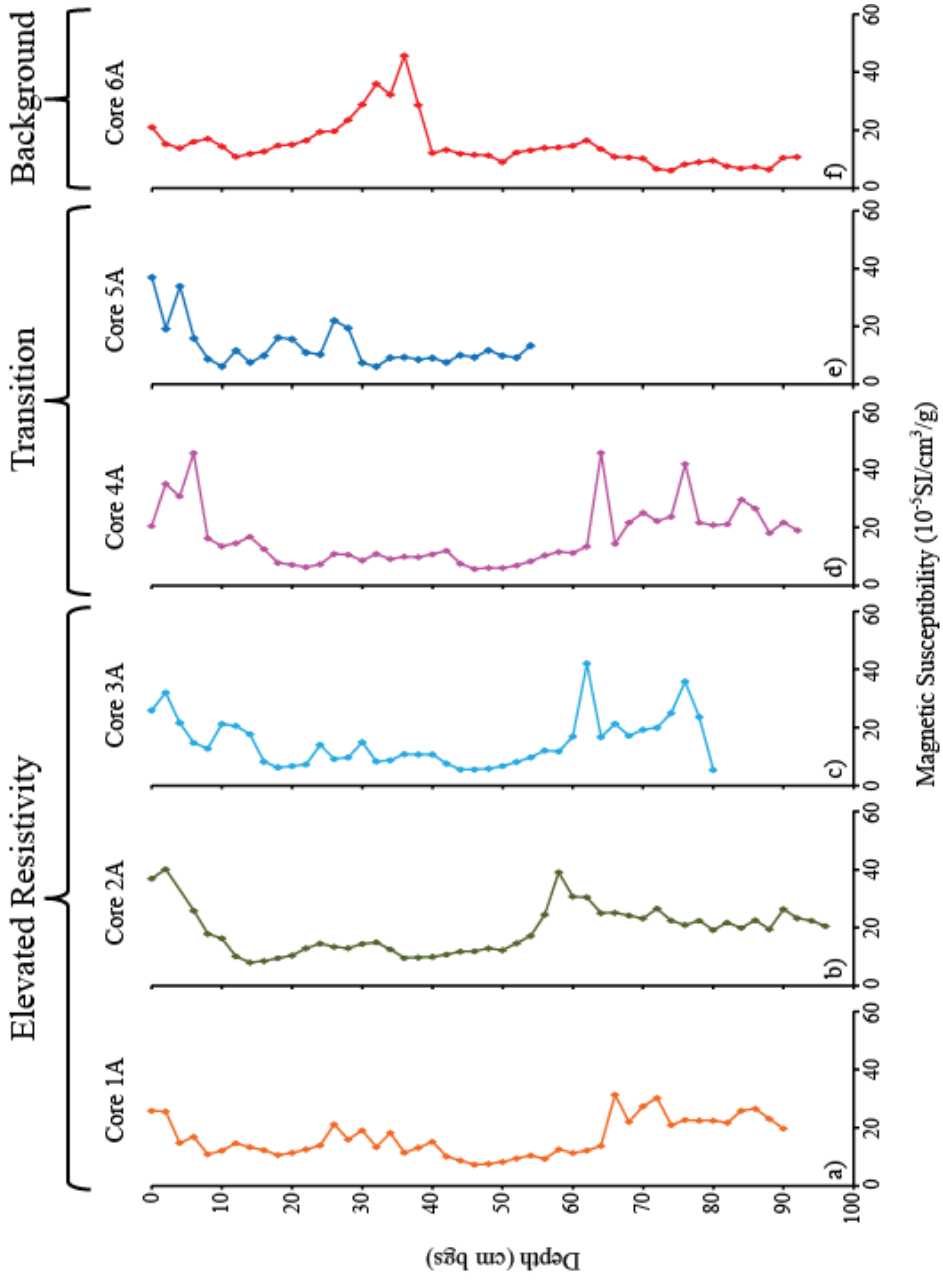

Figure 11. Plots showing variations in magnetic susceptibility with depth for cores sampled.

between depths of 18cm through 54 cm averages 10 (10^{-5} SI/cm^3/g). Core 5A has two distinct peaks at 4 cm and 26 cm of 34 (10^{-5} SI/cm^3/g) and 22 (10^{-5} SI/cm^3/g) respectively (Figure 11e). These variations with depth produce three trends that can be spatially traced through cores in Figure 11. Core 6A, located in the background, shows an increasing MS values beginning at a depth of 12 cm to the largest peak of the core at 36 cm of 46 (10^{-5} SI/cm^3/g) followed by a steep drop in MS over the next 4cm to a depth of 40 cm where it levels out averaging approximately 12 (10^{-5} SI/cm^3/g) (Figure 11f). All cores have elevated MS within the top 10 cm, with cores 4A, 5A, and 2A registering the highest values within that depth range. Cores 1A, 2A, 3A, 5A, and 6A all show an increase in MS within the range of 20 to 45 cm bgs. Cores 1A, 2A, 3A, and 4A display an average increase in MS between the depths 55 to 85 cm

3.3.3 Inorganic and Organic Carbon: Core 6A shows a TOC sharp peak of 3.2 weight percent carbon (W%C) centered around 20 cm bgs while no significant variation was seen in TIC measurements above and below (Figure 12b). TIC is core 1A shows two peaks of 0.71 W%C and 0.94 W%C at 40 cm bgs and 66 cm bgs respectively (Figure 12a). The TOC for core 1A exhibited two peaks (of 1.5W %C and 1.6W %C at depths of 32 cm bgs and 72 cm bgs, respectively as well as an area from 50-58 cm bgs where essentially no TOC (<.07 W%C) was recorded (Figure 12a).

3.3.4 X-Ray Fluorescence: Two zones with elevated concentrations of iron, manganese, and sulfur are represented by the gray boxes cutting through Figure 13a, b, and c. The first zone is located between the depths of 18 cm and 42 cm bgs, while the second is found between the depths of 60 cm to 76 cm bgs. Zones with elevated iron and manganese can be seen in core 2 between the depths 48 cm to 68 cm bgs (Figure 13d and e) as well as two zones within core 3 between the depths of 20 cm to 46 cm bgs and a slightly smaller zone located between 54 cm and 72 cm bgs (Figure 13g and h). All three of these zones in core 2 and core 3 do not show any increase in the concentration of sulfur (Figure 13f and I respectively) at the previously mentioned

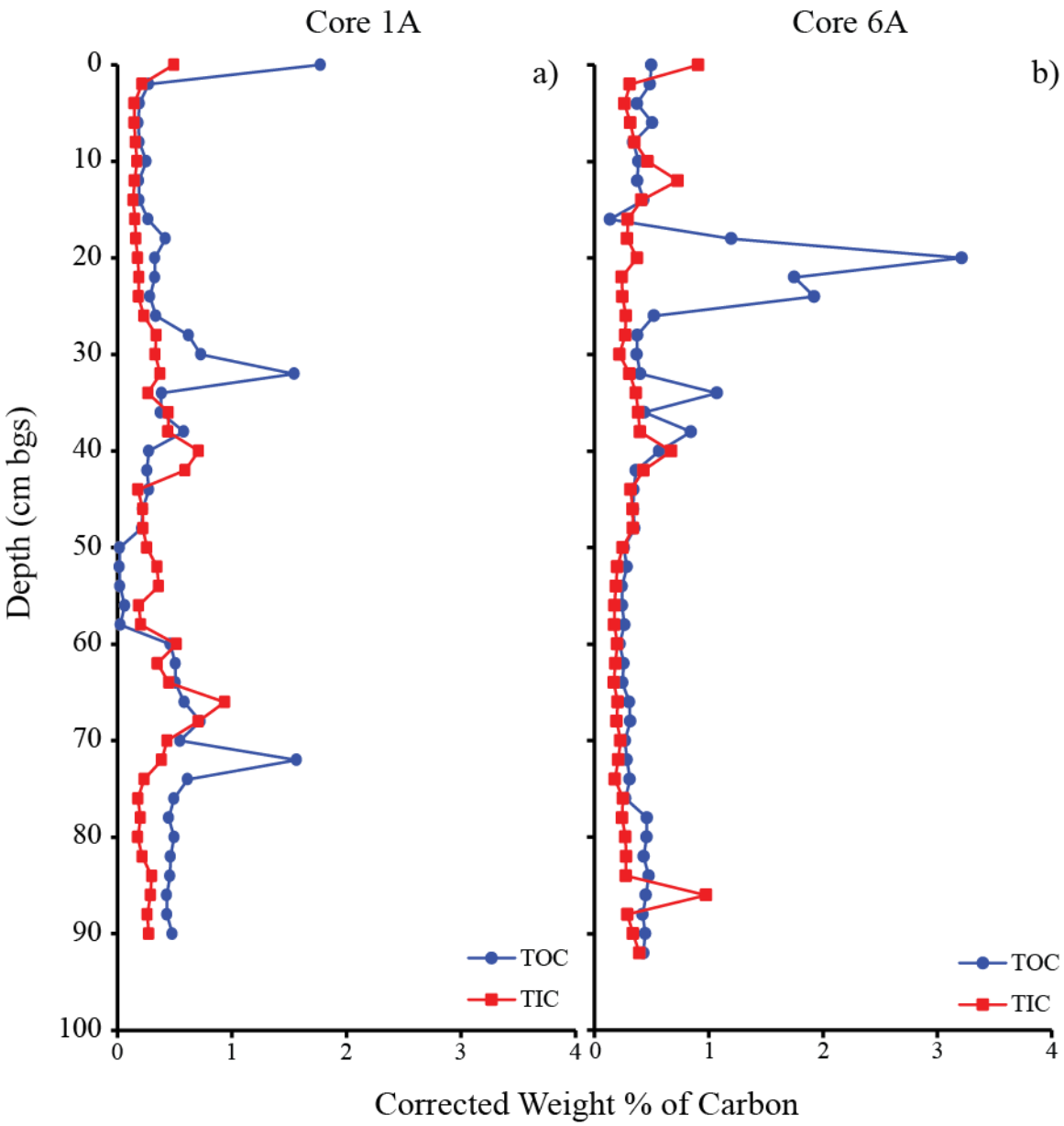

Figure 12. Total organic carbon (TOC) and total inorganic carbon (TIC) for a) core 1A and b)core 6A.

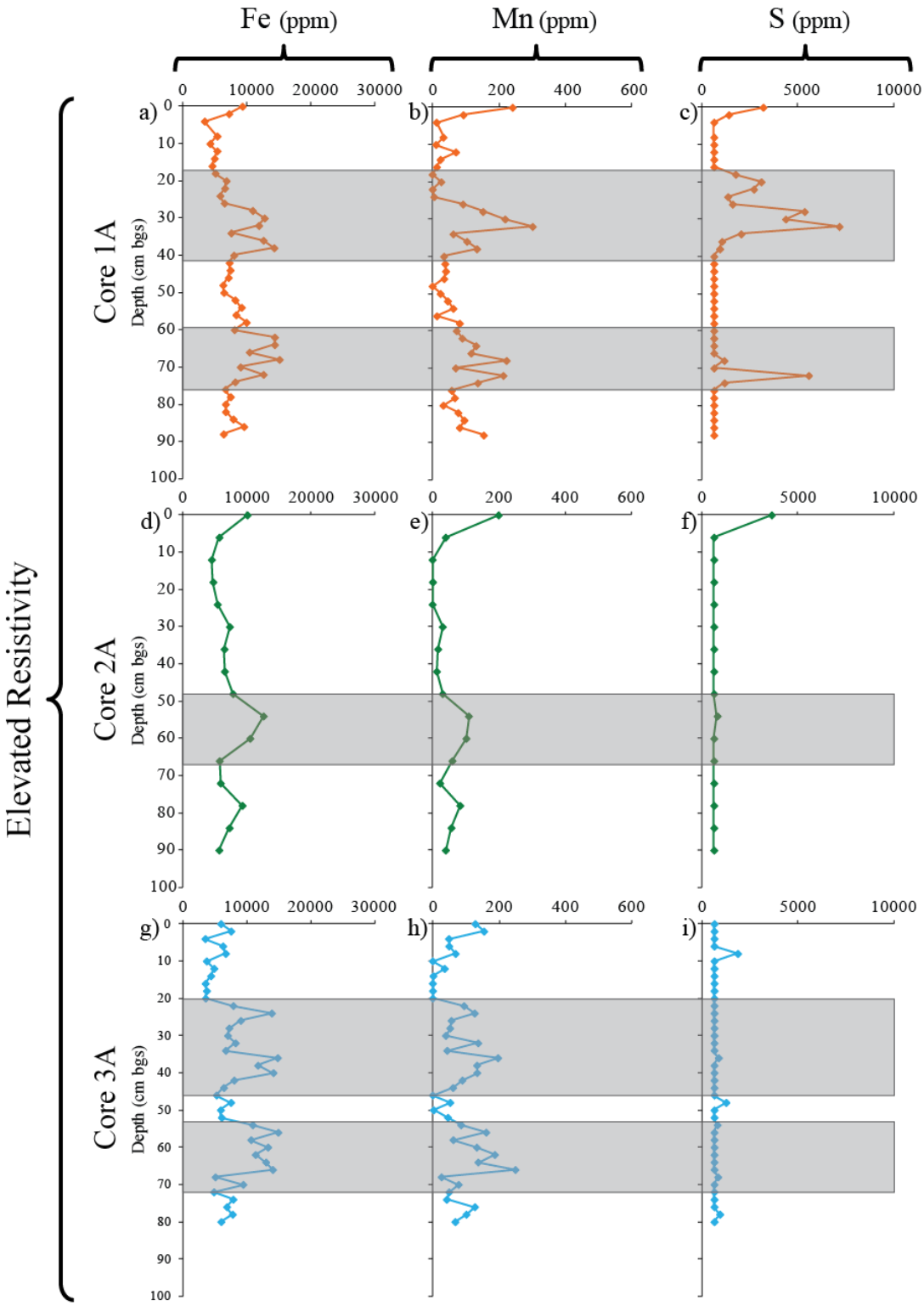

Figure 13. Iron, manganese, and sulfur concentrations determined by x-ray fluorescence for core 1A, 2A, and 3A from within the area of elevated resistivity.

.

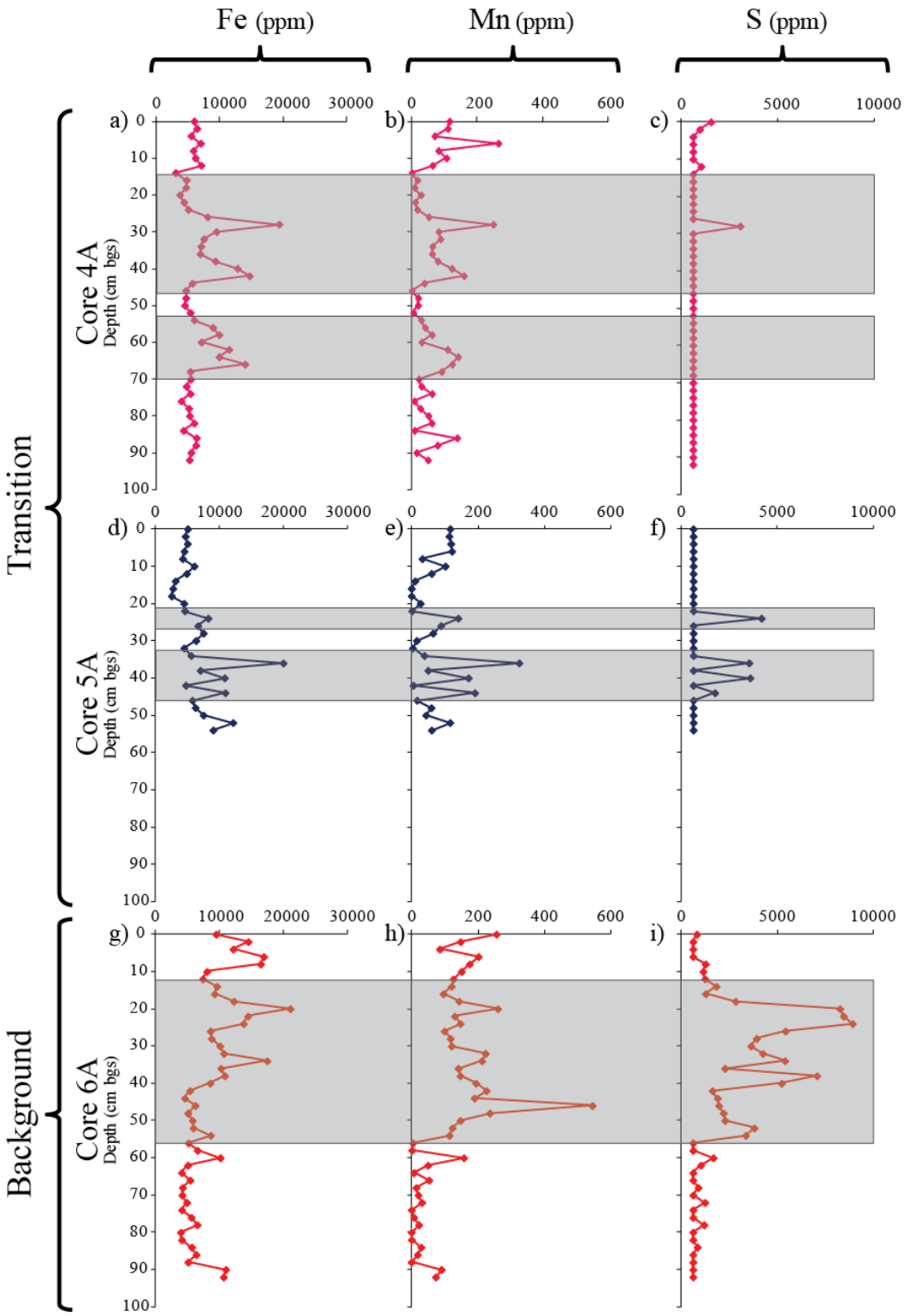

Figure 14. Iron, manganese, and sulfur concentrations determined by x-ray fluorescence for core 4A and 5A from the transitional area and core 6A from the background

depths. Core 4 displays two zones of increased iron and manganese which can be seen between the depths of 14 cm to 48 cm bgs and from 52 cm to 70 cm bgs (Figure 14a and b). While both of these zones are quite large, elevated sulfur concentration is only seen as a quick spike at a depth of 28 cm (Figure 14c). Two smaller zones are seen in core 5, the first is between the depths of 20cm to 28 cm and is characterized by smaller increases in both iron and manganese (Figure 14d and e respectively) while a quick, sharp increase in sulfur is seen just a the depth of 24 cm (Figure 14f). The second zone displays dramatic oscillation of highs and lows between the depths of 32 cm and 46 cm in iron, manganese, and sulfur (Figure 14d, e, and f respectively). Core 6 from the background area shows a broad zone between 12 cm and 56 cm where iron, manganese, and sulfur all display elevated concentrations relative to the rest of the core (Figure 14g, h, and i). The sulfur concentrations (Figure 14i) seen between 20 cm to 24cm bgs are the highest sulfur concentrations seen through the cores sampled at this site.

3.3 Control Experiments

3.3.1 *Oil Saturation*: The experiments investigating the resistivity response due to variations in oil saturation with a premade solution consisting of 30.5 g/l NaCl is presented in Figure 15a. The data shows a very small increase in resistivity (within a narrow range in resistivity) due to a change in the percent of oil saturation (Figure 15a). The true resistivity response of a sample with no crude oil measured at 0.782 Ωm, while the resistivity response of a sample with 20% crude oil saturation measured at 0.944 Ωm (Figure 15a). The percent change of the percent oil saturation was 17.16% with the tested range of 0-20% crude oil saturation

3.3.2 Variations in Salinity: The purpose of this experiment was to gain insight into the relationship between the magnitude of salinity in pore space and the corresponding apparent ER response by creating an equation (Eq. 2) from a linear best fit line, calculated using data from the eight measurements taken within the range of 20-34 mg/l (Figure 15b).

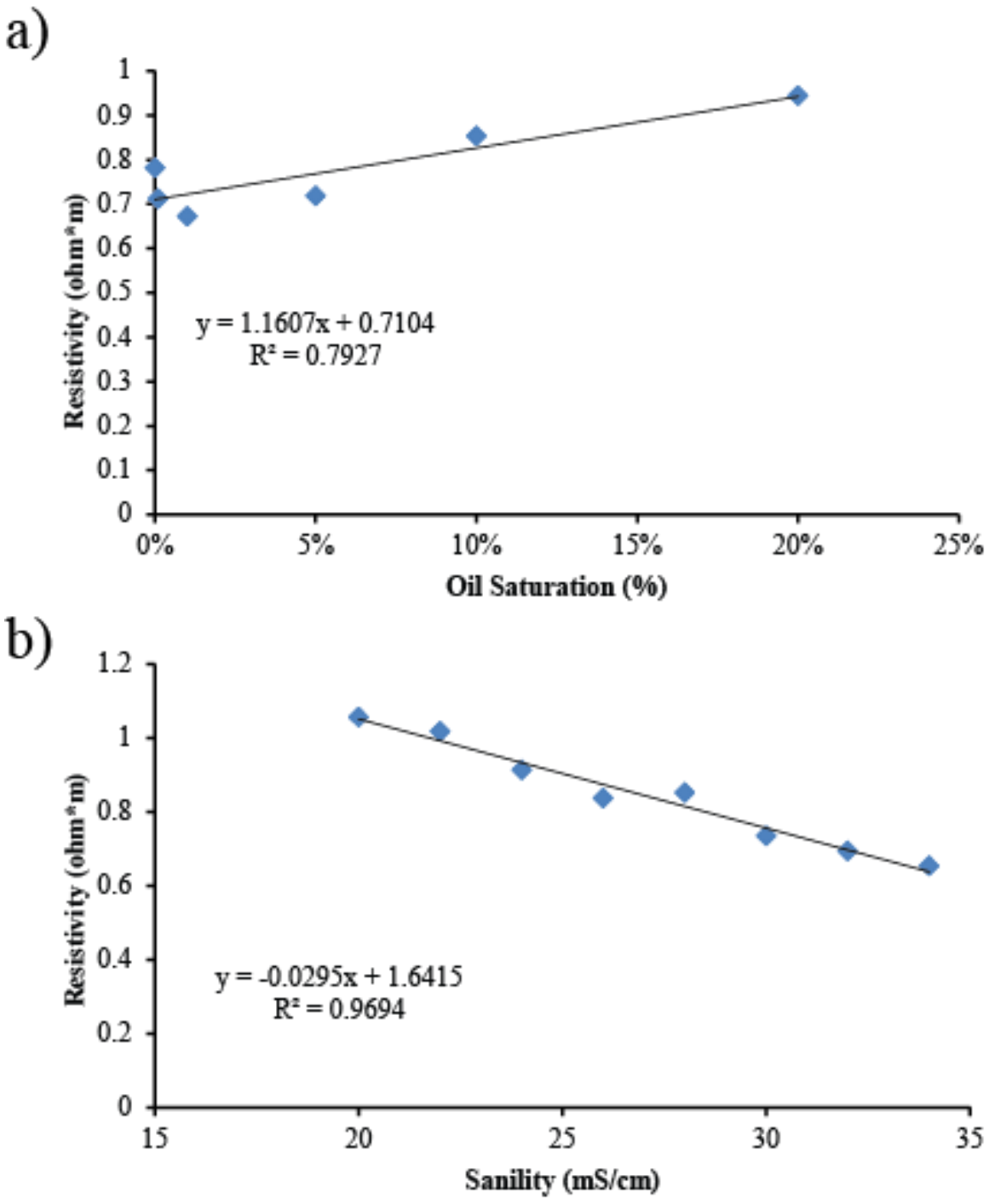

Figure 15. a) Variations in resistivity as function of crude oil saturation at a constant concentration of 30.5g/l NaCl; b) variations in resistivity as a function of salinity concentration.

$$y = -0.0295x + 1.6415 \quad (2)$$

Where *y* is the salinity value and *x* is the apparent resistivity value (post correction with geometric factor). This equation was applied to the 1D depth data of ER line 2 by inputting the apparent resistivity values determined from above as "x" into the y=mx+b equation and solving for *y* yielded a projected salinity range of 10-25 mg/l at well 2 with the lowest values at a depth of 60-85 cm (Figure 16b). The same procedure was done to the 1D depth data of ER line 6 that was nearest well location 1, the projected range was 5-27 mg/l with the lowest values at a depth of 60-85 cm (Figure 16a).

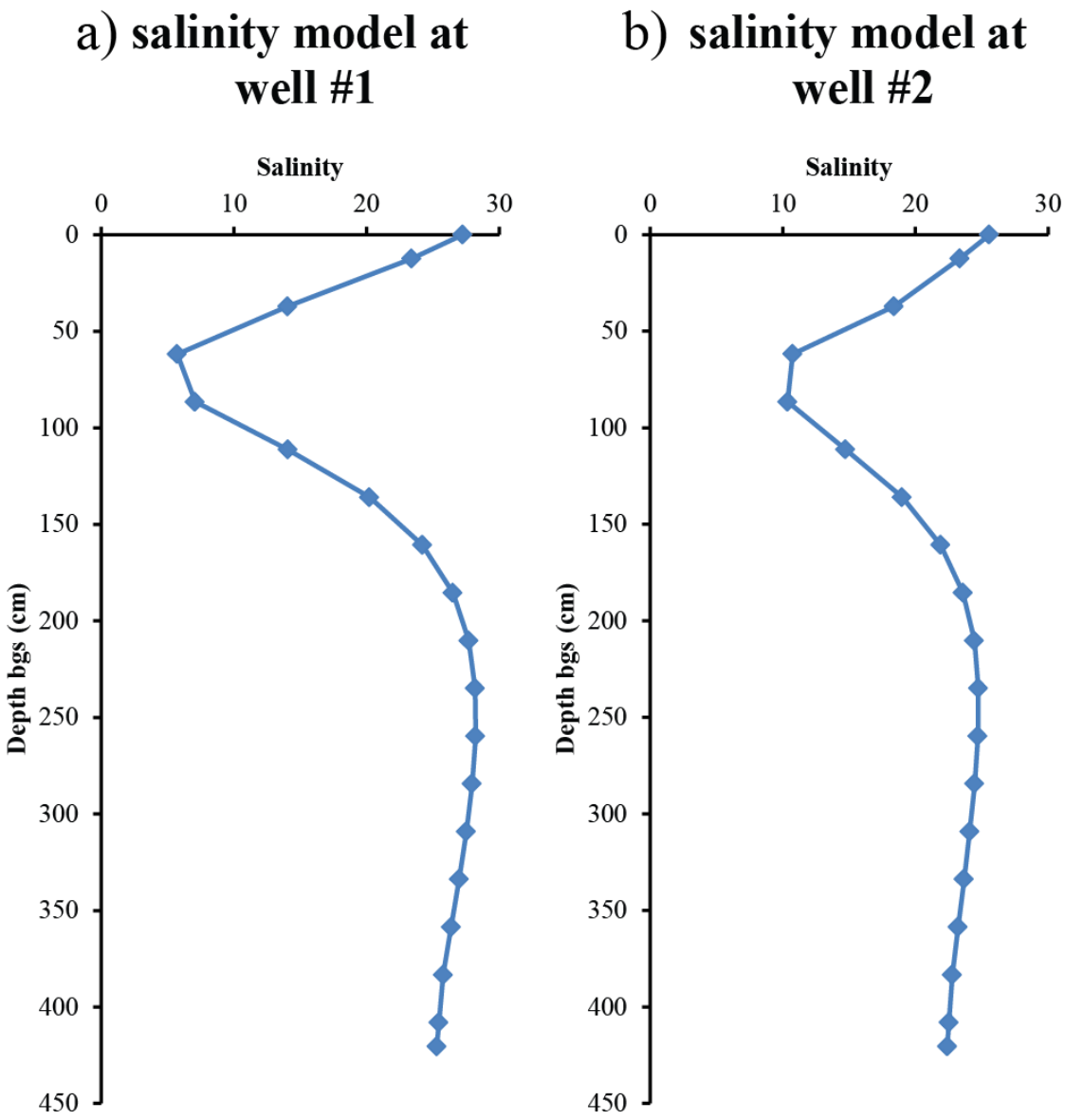

Figure 16. a) b) variations in bulk resistivity converted to salinity values with depth using the equation from Figure 13 b

CHAPTER IV

DISCUSSION

4.1 Electrical Variation: An examination of the geoelectrical images shows that the variation in resistivity is very small and ranges between 0.65-2.5 Ωm. This is expected due to the high salinity and hence high conductivity of the sediments of barrier islands (salinity ranges from 14.07 – 80.98 Mg/L, table 1; Figure 7). Nonetheless, there is a distinct layer ~ 1 m thick found between the depths of 0.25 and 1.20 m that shows slightly elevated resistivities with values > 1.5 Ωm (Figure 4). To assess the lateral extent of this layer, a map of resistivity variations as a function of depth (depth slices) (Figure 5a-d) was produced and compared to EM images at four different frequencies (Figure 6a-d). The resistivity depth slices and EM depth maps show that the relatively higher resistivity (lower conductivity) layer found between the depths of 0.25 and 1.20 m is found within the impacted zone and increases in magnitude and thickness towards the shoreline (to the NW).

A companion study at the site by collaborators at Rutgers University investigated the sensitivity of electrical resistivity on of biogeochemical processes associated with the biodegradation of hydrocarbons in the subsurface using surface and borehole resistivity arrays. Pixel time series analysis of an inverted time sequence of resistivity sections highlighted differing responses between the areas defined in this study as the impacted and transitional areas. The area of elevated resistivity exhibit persistent resistivity decreases over time, whereas the transitional area exhibit relatively uniform resistivity. This information coupled with the presence of hydrocarbon degrading microbes suggests the decrease in the observed electrical response is

thought to be due to the biodegradation of the relatively higher resistivity layer of oil.

4.2 The Presence and Potential Role of Microbes at the Site: A complementary examining the possible presence of microorganisms able to degrade hydrocarbons at the site was completed by Dr. Babu Fathepure's laboratory at Oklahoma State University. Previous investigations have documented the fact that hydrocarbons can be easily degraded under low salinity environments typically found in terrestrial and marine habitats (< 3% salinity) (Le Borgne et al. 2008; Pérez-Pantoja et al. 2010). However, limited studies exist on the degradation of hydrocarbons under high salinity conditions (>10 % salinity) as found in coastal zones and salt marshes as was the case of our field site.

4.3 Microbial Diversity: Analysis of 16S rRNA genes revealed the presence of highly diverse microbial community regardless of oil presence. Important to note is the diversity observed between samples collected in the background and the area of elevated resistivities; the background area provided a more diverse population of microbes, whereas the area of elevated resistivity showed a less diverse population (Figure 17).

4.4 Hydrocarbon Degrading Potential of Microbes found at Site: In addition microcosm experiments set up to investigate the hydrocarbon degrading potential showed that benzene and toluene in microcosms prepared with soil/sediment samples collected from the impacted zone were completely degraded within 2 weeks (Figure 18). Subsequent addition of the hydrocarbons to these samples resulted in an increased rate of degradation with complete degradation occurring within 7 days suggesting that enrichment of hydrocarbon degrading microorganisms had occurred (Figure 18). Surprisingly, experiments with samples from the background location showed negligible amount of benzene and toluene degradation in 3 weeks, despite the fact that the microbial diversity results suggested the presence of hydrocarbon degrading microorganisms (Figure 18).

4.5 Presence of High Saline Hydrocarbon Degrading Genes: The study also tested for the presence of important hydrocarbon-degrading genes such as catechol 1, 2-dioxygenase (1, 2-CTD) and

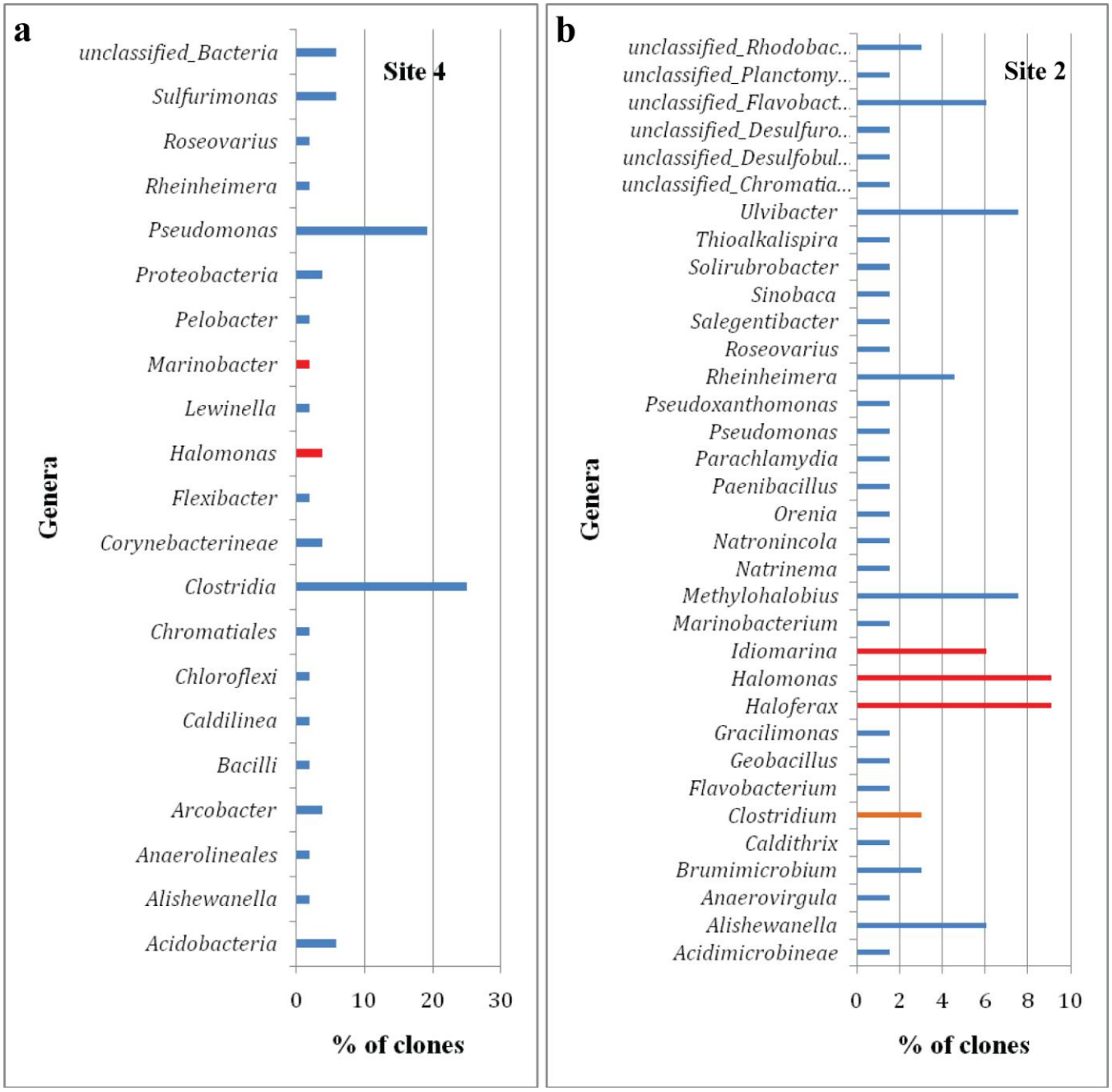

Figure 17. a) Microbial community composition within the the area of elevated resistivity. Members of *Pseudomonas* sp. dominated the community (20% of clones). Many *Pseudomonas* strain have the capacity to degrade petroleum compounds. Analysis also included the presence of *Marinobacter* sp. and *Halomonas* sp. members of these genera are known hydrocarbon degraders at high salinity. b) Microbial community composition within the background area is much more diverse then the area of elevated resistivity. Multiple hydrocarbon degrading halophlic organisms seen within the area of elevated resistivity are also present in the background, including *Marinobacter* sp. and *Halomonas* sp

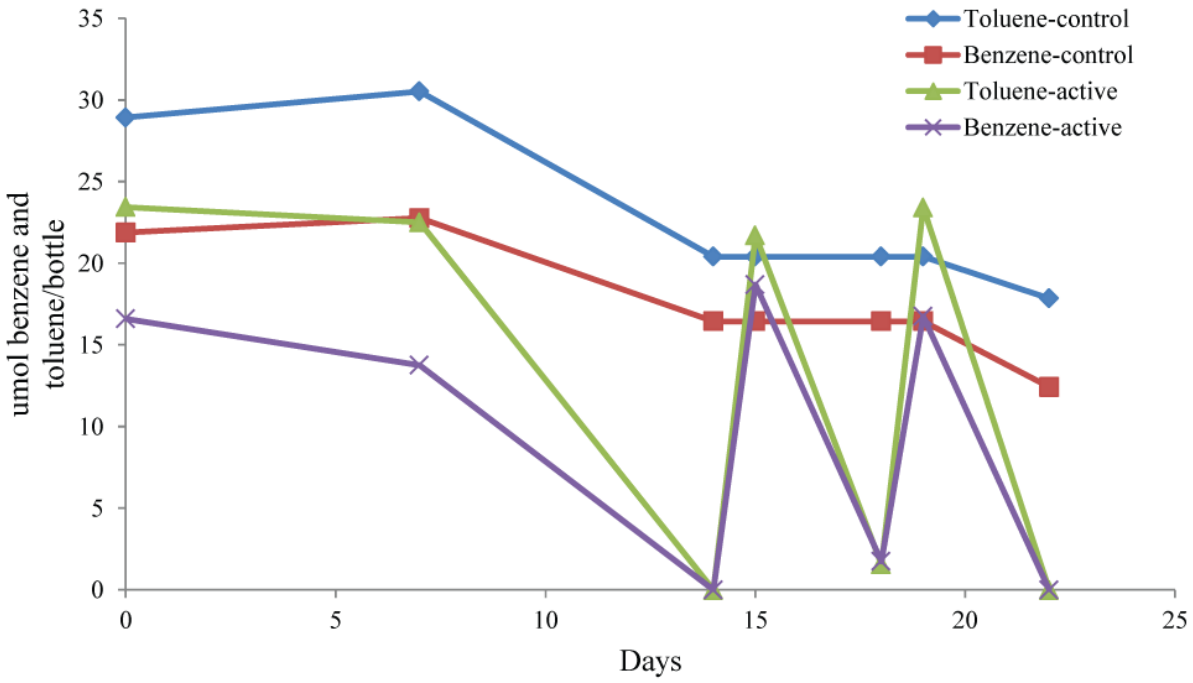

Figure 18. Biodegradation of hydrocarbons from soils extracted from within the area of elevated resistivity. Benzene and toluene degrade quickly in active bottles compared to autoclaved bottles suggesting biological degradation

protocatechuate 3, 4-dioxygenase (3, 4-PCA) in all samples collected. The data showed the presence of these conserved genes in all samples collected from the area of elevated resistivity suggesting the genetic potential of hydrocarbon degradation by native microorganisms. However, no genes were detected in samples collected from sites considered background. Finally, further experiments to determine the hydrocarbon degradation potential under high salinity conditions (up to 15% salinity) showed that *Marinobacter* dominated the community representing >80% of clones. *Marinobacter* sp have been isolated from various hydrocarbon-contaminated high salinity environments (Berlendis et a. 2010; Duran, 2010) as well as from BP oil –impacted beach sands collected from Pensacola Beach, FL (Kostka et al. 2011). .Although it is not possibly to conclusively determine that the high resistivity layer is due to the presence of the oil, the microbial results suggest that our impacted zones had native microbial populations capable of degrading aromatic hydrocarbons at salinities ranging from 6 to 15 % NaCl.

4.6 Electrical Properties of the Pore Space: In order to gain insight into what is causing this electrical anomaly, we use Archie's Law (1942), which in the absence of clays, describes the bulk conductivity of consolidated sediment. First we evaluate the effect of spatial variation in grain size (lithology) on the electrical response. Figure 11 suggests that the grain size throughout the entire site is a mixture of medium, fine, and very fine sand grains, with little clay or silt detected. The electrical conductivity is related to the particle size by the electrical charge density at the surface of the solid constituents (Samouëlian et al. 2005). In clay soil, the electrical charges located at the surface of the clay particles produce a greater electrical conductivity than in more coarse-textured soils like sand due to the magnitude of the specific surface area (Samouëlian et al. 2005). Within the anomalous area the grain size is dominated by fine grain sand with little to no evidence coarse grain particles. Due to the lack of lithographic variations the electrical charges produced by an increase in coarse grain sediments can be ruled out as a potential factor contributing to the electrical anomaly observed. The resistivity anomaly occurred within an interface where the sediments appeared fully saturated, although do to the high microbial presence and geochemical measurements, the production of gas derived from organic matter

degradation could be used to explain the variations in the bulk resistivity The electrical properties of the pore fluid could also be a controlling factor in the generation of the increased apparent resistivity anomaly observed in the area of elevated resistivity due to dynamic ranges seen through the site in the aqueous geochemistry data.

4.7 Electrical Response to Variations in Percent Oil Saturation: To assess if the 1.2 to 2.3 Ωm resistivity layer was due to the presence of oil, we conducted a controlled experiments to determine how much oil saturation would be required to explain the resistivity data. The data collected from the column experiments that measured the resistivity response due to variations in the percent of oil saturations were compared to the apparent resistivity values from the post inversion 2D lines collected at the site. This was to predict what the percent oil saturation values would be expected in our extracted cores in order to produce the values associated with the relatively higher resistivity layer observed through the area of elevated resistivity. The results suggest that the 1.2 to 2.3 Ωm range of apparent resistivity as observed in L2 and L6 at a depth of 0.25 to 1.25 m (Figure 4a and 4d) would be due to hydrocarbon saturation greater than 20%. In order to determine if the oil was strongly sorbed to the sand grains, sediment samples were sent off to labs for TPH analysis. While all samples came back BPQL, only one sample was extracted within the depth range that the electrical anomaly is found throughout the site: S#1-12 was the deepest sample extracted at a depth of 0.3048 m bgs.

4.8 Electrical Response to Variations in Salinity: Because the geochemistry is unable to fully support the presence of hydrocarbons at the depth where the apparent resistivity anomaly was observed, an alternative explanation was pursued using variations in the salinity measured at the site. Applying the salinity equation (Eq.2) determined by measuring the resistivity response to variations in salinity to the measured salinity range 14.07 to 38.21 mg/L of wells within the impacted and transitional areas (W1, W2, and W3) produces a proposed apparent resistivity range of 0.51 to 1.23Ωm. Therefore, variations in salinity could potentially produce a plausible explanation as a controlling factor in the generation of the increased apparent resistivity anomaly seen in the area of elevated resistivity. The salinity range over the

entire site is 14.07 through 80.98 units and is caused by the extremely diverse hydrologic environment of a barrier island. Precipitation rates and tidal variations; including the tidal height and infiltration rates would change the spatial distribution of salinity in the near subsurface therefore altering the electrical response of the fluid.

4.9 Interpretation of Geochemical Data: In saturated sediments contaminated with hydrocarbon, the reduction of the contaminant mass by microbes can be determined by the presence of multiple factors: 1) microbes capable of degrading the hydrocarbon, 2) terminal electron acceptors processes (TEA's), 3) production of by-products of hydrocarbon degradation such as organic acids (Cozzarelli et al., 1990), 4) the production of carbon dioxide (Sauck 2000) and 5) the shifts in the isotope ratio of dissolved inorganic carbon (DIC) (Aggarwal and Hinchee, 1991).

The geochemical data within the site suggest the contamination of the groundwater may have been in the dissolved form. Depth profiles show evidence of biodegradation of organic carbon; DIC concentrations within the area of elevated resistivity were found to be relatively lower, with values between 204 to 480 mg CO_2/l at depths of 10 to 100 cm compared to the background area with values between 730 to 2340 mgCO_2/l from depths between 25 to 125 cm. W1 and W2 within the area of elevated resistivity show higher dissolved Fe(II) and Mn (between the depths 0.50-1.20 m bgs) compared to the background indicating reduction of Fe(III) and Mn (IV) from solids coupled to microbially mediated degradation (Atekwana et al., 2005) was greatest within the area of elevated resistivity. In vertical profiles, the depths with higher Fe(II) and Mn coincide with the location and depth of the resistive anomaly seen in ER line 2 (Figure 4a). Variability and lower values of NO_3^- and SO_4^{-2} in the vertical profiles for W1 and W2 are most likely due to utilization by microbes during the degradation of organic matter. W4 in the background area shows relatively low pH values compared to the area of elevated resistivity; this can be due to an accumulation of organic acids produced from decomposition of organic material from microbial activity.

4.10 X-Ray Fluorescence: The presence of tar layers near the shoreline were considered when initially choosing the field site. Although no such tar layers were visually observed for the area of elevated resistivity, the area had a dark coloration on the surface (Figure 19a); a dark layer seen between the depths of 20 cm to 45 cm bgs (Figure 19b) was seen in the sediment in the extracted cores within the area of elevated resistivity. Due to the depth of this layer and the visual representation of a smear zone (Figure 19c) it was initially believed that this layer was the cause of the zone of higher resistivity of the ER lines within the area of elevated resistivity and was caused by either hydrocarbon deposited by the tides, the product of biodegradation of petroleum hydrocarbon, or potentially organic matter degradation coupled to sulfate and iron reduction. The elevated concentrations of iron, manganese, and sulfur seen between seen between 20 cm to 44cm bgs in core 1A (Figure 20a, b, and c respectively), the increase in TOC content seen in core 1A (Figure 20e) at the same depths, depleted DO values seen at 25 cm bgs in W1 (Figure 20d), and the strong presence of hydrocarbon degrading microbial gene suggests the presence of sulfate reducing bacteria (SRB) (Chapelle and Lovley 1992). The black layer at approximately 30-32 cm bgs in core 1A correlates perfectly to the large manganese and sulfur spikes from the XRF, as well as the TOC (Figure 20b, c, and e respectively), further supporting that the black layer seen in core 1A is due to the active biodegradation of the soils in response to increased carbon loading, potentially from spill hydrocarbons.

Core 6A from the background area displays (although sporadic with depth) elevated concentrations of iron, manganese, sulfur, and DO from 12 cm to 56 cm bgs (Figure 20f, g, h, and i respectively). The sulfur peak seen at 20 cm to 24 cm bgs in core 6A correlates to the TOC spike seen at 20 cm bgs (Figure 20j). The increased concentrations in iron, manganese, sulfur, and TOC in core 6A can be interpreted as the product of SRB, yet the abundance of dissolved oxygen within the same depth interval reveals that although SRB degradation may have taken place, it was not active during the time when water samples were collected (Chapelle and Lovley 1992).

Figure 19. a) Field photograph of impacted area showing darker sands. b) Core from within the impacted area displaying the darker layer or smear zone between the depths of 0.15m to 0.45m bgs. c) depth profile of the smear zone in a trench

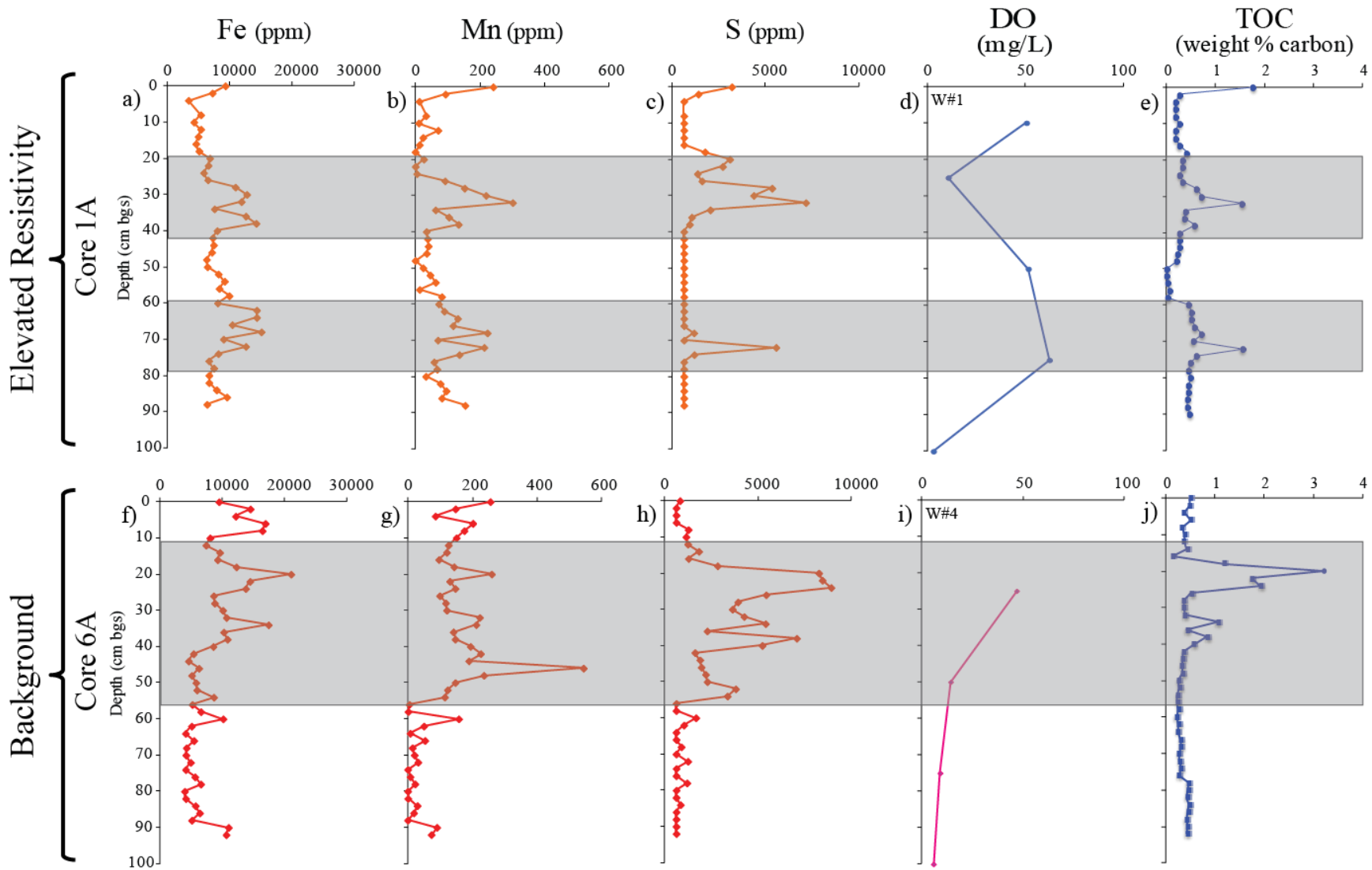

Figure 20. Iron, manganese, and sulfur concentrations from cores 1A and 6A are compared with dissolved oxygen (DO) and total organic carbon (TOC) concentrations

4.11 Crude Hydrocarbon Contamination due to Natural Oil Seeps: Although, the presence of oil cannot be conclusively demonstrated at the site, the microbial population data points to the fact that the exposure of the site to oil from the BP spill or some previous spills had resulted in the enrichment of native populations capable of degrading oil within the area of elevated resistivity. This can be explained by comprehensive remote sensing surveys indicate that there are approximately 350 constant oil seeps in the Gulf of Mexico (MacDonald and Leifer 2002), of these, 63 individual seeps were identified using multiple data sets as perennial oil slicks (MacDonald et al., 1996). Seep rates were calculated to give a total Gulf of Mexico seep rate of about 140,000 metric tons (~42 million gallons) per year and a seep rate of 73,000 metric tons (~21.9 million gallons) per year for just the northern Gulf of Mexico (Kvenvolden and Cooper 2003) where this research's site is located. The lack of the enrichment of native populations of oil degrading microbes at the background site suggests an absence of significant quantities of oil in the background site. This could be the result of a range of scenarios: rapid degradation possibly enhanced by the dispersants used by BP at the Maconda well site, or possibly the general lack of infiltration of contaminant as far inland as the background area.

4.12 Evidence of Rapid Degradation of Hydrocarbon: The majority of petroleum hydrocarbons are hydrophobic; causing any biodegradation to take place at the hydrocarbon – water interface, therefore the ratio between surface area to the volume of the oil to significantly impact the rate of biodegradation (Atlas and Hazel, 2011). The use of a chemical dispersant to increase emulsification of the oil slick improves bioavailability of the contaminant and has been shown to enhance oil biodegradation (Wolfe et al., 1998). Another variable influencing the intensity of biodegradation is temperature, an increase results in a decrease in viscosity, thereby affecting the degree of distribution, and an increase in diffusion rates of organic compounds (Margesin and Schinner, 2001). Therefore, at the elevated temperature range (23.87 to 33.69°C)

observed within the area of elevated resistivity one would expect higher reaction rates will occur due to smaller boundary layers (i.e. increased solubility).

Independent laboratory test results for the presence of hydrocarbons are inconclusive. This could be attributed to several possible scenarios, one being the sampling depth for the presence of hydrocarbons, was shallower (<35 cm) whereas, the dark layer seen in extracted cores extends to a depth greater than 0.45m (Figure 14b). Nonetheless, non-detect levels of hydrocarbon could be explained in terms of rapid biodegradation of the oil if the site was originally contaminated. Other recently published studies have suggested very rapid rates of degradation of the crude oil in the area of this researches site. Water samplings performed by Allen et al. (2012) show the highest amounts of PAH detected were recorded by samplers in the water column during heavy shoreline oiling in the month of June. This was followed by a sharp decrease in concentration during August and September and the measurements had approximately returned to pre-oil spill concentrations by March 2011. This is complemented by research showing that upwards of 40% of the oil was lost in the water column between the wellhead and the surface as a result of dissolution and mixing as the oil moved through the water column towards the surface (OSAT 2011).

Geochemical data for this study was obtained in the field May 2012, after the research by Allen et al (2012) found the area to be back to pre-oiling conditions. This information could be used to explain the absence of detectable TPH from the water samples that were collected January 11th, 2011 and sent out to an independent lab for analysis.

CHAPTER V

CONCLUSION

The BP *Deepwater Horizon* oil spill provided an unprecedented opportunity to characterize and delineate the crude oil, as well as capture the early time biogeophysical signals resulting from the physical, chemical, and microbial degradation of the crude oil in a highly saline environment, aiding in the development of models that describe the evolution of biogeophysical signals from a young to more mature crude spills. In this paper, we interpret the geophysical results within the constraints of the biological and geochemical data acquired in order to better understand the geophysical signature of a fresh crude oil in a saline environment.

The main results and discussion are listed in the following bullets:

- Electric methods show a distinct layer ~ 1 m thick found between the depths of 0.25 and 1.20m that shows slightly elevated resistivities with values > 1.5 Ωm.
- Further examination of the geoelectrical images shows that the variation in resistivity is very small and ranges between 0.65-2.5 Ωm. This is expected due to the high salinity and hence high conductivity of the barrier island.
- The presence of microbes capable of hydrocarbon degradation could where found in all areas of the site.
- Only the samples collected from the area of elevated resitivity displayed the genes for active degradation while the samples from the background area were dormant even when spiked in microcosm experiments.

- The presence of the microbes suggests that oil has been present at the site, the experiments cannot determine the time at which the oil was present as well as the character of the oil. The reason for the enrichment of hydrocarbon degrading microbial genes at the site is further supported if the presences of oil from natural oil seeps are taking into account.
- Elevated DIC, sulfate, and higher dissolved Fe(II) and Mn found within the area of elevated resistivity between the depths of 0.25 to 1.25m bgs are indicative of hydrocarbon contamination, these could also be explained by the degradation of non-hydrocarbon organic matter; supported by the depletion of TOC seen in core 1A between 50 cm to 58 cm bgs.
- Increased variability and lower values of NO_3^- and SO_4^{-2} in the vertical profiles for W1 and W2 are most likely due to utilization by microbes during the degradation of organic matter.
- It is unlikely to know how the site geochemically evolved through time as only one set of geochemical data was acquired, making it difficult to differentiate between data that supports hydrocarbon degradation versus the background, or pre-oiling environment of the barrier island.
- Elevated iron, manganese, sulfur, and TOC from core 1A, coupled with depleted DO concentrations from W1, between the depths of 20 cm to 44 cm bgs are indicative of hydrocarbon degradation by sulfate reducing bacteria. This is further supported by the high concentration of microbes capable of hydrocarbon degradation found within the area of elevated resistivity and the presence of black sands from possible iron sulfide precipitation.

- The electrical response seen within the area of elevated resistivity could be explained by the production and ebullition of gas in the sub surface by the degradation of hydrocarbon by sulfate reducing bacteria.
- All soil and water samples sent out to independent laboratories to test for the presence of hydrocarbons came back below practical quantitative limit. This could be explained by extremely rapid levels of degradation of crude oil in the area of this research.
- The application of the salinity equation to the measured salinity range of wells within the impacted and transitional areas (W1, W2, and W3) produced an apparent resistivity range of 0.51 to 1.23 Ωm. While this range is not an exact match to the range seen in the 2D ER lines, the lab experiment only took into consideration variations in salinity and their effects on resistivity. This is not to say that other physical, chemical, and biological processes cannot influence the range of apparent resistivity values.
- This research site can be characterized as having low organic content, moderately low total porosities, and high hydraulic conductivities (Lisle and Comer, 2011). These conditions provide an environment that is capable of rapid and efficient degradation of low to moderate concentrations of crude oils without nutrient and or oxygen enhancement.
- The rate of degradation was also affected by the dispersants ability to alter the inherent chemical and physical properties of oil, allowing the microbes to digest hydrocarbon more quickly (Atlas and Hazen 2011).
- With the seawater containing adequate concentrations of oxygen and nutrients to facilitate microbial degradation of crude oil, coupled with wave action driving into and flushed out of the pore spaces of the sediments, an elevated rate of biodegradation is produced (Lisle and Comer, 2011).

Based on the geochemical, microbial, and soil analysis, the relatively higher apparent resistivity anomaly observed between the depths of 0.25 m to 1.20 m bgs could be explained by two scenarios. The first and most likely explanation is the area of elevated resistivity was caused by the ebullition of gas in the subsurface produced by the degradation of petroleum hydrocarbon or some other organic matter coupled to sulfate and iron reduction. Due to inconclusive test results for the presence of hydrocarbons from independent laboratories, analysis into the electrical response derived from variations in salinity produced a resistivity range very similar to that seen throughout the site. Further research is needed

REFERENCES

Abdel Aal, G. Z. E. A. Atekwana, L. D. Slater, and E. A. Atekwana, 2004, Effects of microbial processes on electrolytic and interfacial electrical properties of unconsolidated sediments: Geophysical Research Letters, **31**, L12505.

Aeppli, C., Carmichael, C. A., Nelson, R. K., Lemkau, K. L., Graham, W. M., Redmond, M. C., Valentine, D. L., Reddy, C. M., 2012, Oil Weathering after the Deepwater Horizon Disaster Led to the Formation of Oxygenated Residues: Environ. Sci. Technol., **46**, 8799-8807.

Allan, S. E., Smith, B. W., Anderson, K. A., 2012, Impact of Deepwater Horizon Oil Spill on Bioavailable Polycyclic Aromatic Hydrocarbons in Gulf of Mexico Coastal Waters: Environ. Sci. Technol. **46**, 2033-2039.

Archie, G.E., 1942. The electrical resistivity log as an aid in determining some reservoir characteristics. Tran. AIME 146, 54–67..

Aggarwal, P.K. and Hinchee, R.E., 1991, Monitoring in situ biodegradation of hydrocarbons by using stable carbon isotopes: Environ. Sci. Technol., **25**(6), 1178-1180

Atekwana, E. A. W. A. Sauck, Werkema, D.D., 1998, Characterization of a complex refinery groundwater contamination plume using multiple geoelectric methods: Proceedings of the Symposium on the Application of Geophysics to Engineering and Environmental Problems (SAGEEP 1998), Environmental and Engineering Geophysical Society, 427-436.

Atekwana, E. A., and R. V. Krishnamurthy, 1998, Seasonal variations of dissolved inorganic carbon and δ13C of surface waters. Application of a modified gas evolution technique: Journal of Applied Geophysics, **205**, L23603.

Atekwana, E. A. W. A. Sauck, and D. D. Werkema, 2000, Investigations of geoelectrical signatures at a hydrocarbon contaminated site: Journal of Applied Geophysics, **44**, 167– 180.

.

Atekwana, E. A., E. A. Atekwana, F. D. Legall, and R. V. Krishnamurthy, 2004a, Field evidence for geophysical detection of subsurface zones of enhanced microbial activity: Geophysical Research Letters, **31**, L23603.

Atekwana E. A, D. D. Werkema, J. W. Duris, S. Rossbach, E. A. Atekwana, W. A.Sauck, D. P. Cassidy, J. Means, and F. D. Legall, 2004b, In-situ apparent conductivity measurements and microbial population distribution at a hydrocarbon contaminated site: Geophysics, **69**, 56-63.

Atekwana, E. A. E. A. Atekwana, R. S. Rowe, D. D. Werkema, and F. D. Legall, 2004c, Total dissolved solids in groundwater and its relationship to bulk electrical conductivity of soils contaminated with hydrocarbon: Journal of Applied Geophysics, **56**, 281-294.

Atekwana E. A, E. A. Atekwana, D. D. Werkema J. P. Allen L. A. Smart, J. W. Duris, D.P., Cassidy, W. A. Sauck, and S. Rossbach, 2004d, Evidence for microbial enhanced electrical conductivity in hydrocarbon-contaminated sediments: Geophysical Research Letters, **31**, L23501.

Atekwana, E. A, Slater, L. D., 2009, Biogeophysics: A New Frontier in Earth Science Research: Reviews of Geophysics, **47**, RG4004

Atekwana, E. A., Atekwana, E. A., 2009a, Geophysical Signatures of Microbial Activity at Hydrocarbon Conatminated Sites: A Review: Surv. Geophys., **31**, 247-283.

Atekwana, A. E., Fonyuy, E. W., 2009b, Dissolved inorganic carbon concentrations and stable carbon isotope ratios in streams polluted by variable amounts of acid mine drainage: Journal of Hydrology, **372**, 136-148.

Atekwana, E. A., E. A. Atekwana, F. D. Legall, R. V. Krishnamurthy, 2005,Biodegradation and mineral weathering controls on bulk electrical conductivity in a shallow hydrocarbon contaminated aquifer: Journal of Contaminant Hydrology, **80**, 149-167.

Atlas, R. M., Hazen, T. C., 2011, Oil Biodegradation and Bioremediation: A Tale of the Two Worst Spills in U.S. History: Environ. Sci. Technol., 45(16), 6709-6715.

Benson, A.K., Pyne, K.L., Stubben, M.A., 1997, Mapping groundwater contamination using dc resistivity and VLF geophysical methods – A case study, Geophysics, vol. 62, pp. 80-86.

Berlendis. S., J-L.Cayol., F. Verhé., S. laveau., J-L. Tholozan., D. Ollivier., R. Auria., 2010, First Evidence of Aerobic Biodegradation of BTEX Compounds by Pure Cultures of *Marinobacter*. Appl Biochem Biotechnol. **160**, 1992-1999

Camilli, R.: Reddy, C.M.; Yoerger, D. R.; Van Mooy, B.A.A.; Jakuba, M. V.; Kinsey, J. C.; McIntyre, C. P.; Sylva, S. P.; Maloney, J. V., 2010, Tracking hydrocarbon plume transport and biodegradation at Deepwater Horizon. Science, 330, 201-204.

CEDRE 2010, Oil spill, Chronological classification, Centre of Documentation, Research and Experimentation on Accidental Water Pollution (CEDRE), 29218 BREST CEDEX 2 France, viewed 1st, September, 2012, <*http://www.cedre.fr/en/spill/chronological-classification.php*>.

Chapelle, F. H., Levley, D. R., 1992 Competitive Exclusion of Sulfate Reduction by Fe(III)-reducing Bacteria: A Mechanism for Producing Discrete Zones of High-Iron Ground Water: Ground Water, **30**(1), 29 – 36.

Che-Alota, V., Atekwana, E. A.,E. A. Atekwana, Sauck, W. A., Werkema, D. D., 2009 Temporal geophysical signature from contaminant-mass remediation: Geophysics, **74**, B113-B123

Conatser, W. E., 1971. Grand Isle: A Barrier Island in the Gulf of Mexico, Geological Society of AmericaBulletin, **82**, 3049-3068

Cozzarelli, I.M., Eganhouse, R. P., and Baedecker, M.J., 1990, Transformation of monoaromatic hydrocarbons to organic acids in anoxic groundwater environment: Environ. Geol. Water Sci., **16**, 135-141

Duran, R. 2010, Marinobacter. P. 1726-1735. *In* K. N. Timmis (ed.), Handbook of Hydrocarbon and Lipid Microbiology. Springer-Verlag, Berlin Heidelberg

Edwards, B. R., Reddy, C. M., Camilli, R., Carmichael, C. A., Longnecker, K., Van Mooy, B. A.S., 2011, Rapid microbial respiration of oil from the Deepwater Horizon spill in offshore surface waters of the Gulf of Mexico: Environ. Res. Lett., **6**, 035301

Eganhouse, R. P., Calder, J. A., 1976, The solubility of medium molecular weight aromatic hydrocarbons and the effects of hydrocarbon co-solutes and salinity: Geochim Cosmochim Acta, **40**, 555-561

Ellwood, B. B., F. B. Harrold, et al. (2004). "Magnetic susceptibility applied as an age–depth–climate relative dating technique using sediments from Scladina Cave, a Late Pleistocene cave site in Belgium." Journal of Archaeological Science, **31**(3), 283-293.

Environmental Response Management Application (ERMA) Deepwater Gulf Response, viewed 30th, August 2012 <*http://www.gomex.erma.noaa.gov*>

The Federal Interagency Solutions Group: Oil Budget Calculator Science and Engineering Team, 2010. *Oil Budget Calculator Technical Documentation*. http://restorethegulf.gov/-sites/default/files/documents/pdf/OilBudgetCalc_Full_HQ-Print_111110.pdf (accessed August 15, 2012)

Fonyuy, E.W. and Atekwana E.A., 2008a. Effects of acid mine drainage on dissolvedinorganic carbon and stable carbon isotopes in receiving streams. Appl. Geochem. 23, 743-764.

Godio, A., Arato, A., Stocco, S., 2010, Geophysical characterization of a nonaqueous-phase liquid-contaminated site: Environmental Geosciences, v.17, p. 141-161.

Gong, C., Milkov, A.V., Grass, D., Sullivan, M., Searcy, T., Dzou, L., Depret, P., 2010, The significant impact of weathering on MC252 oil chemistry and it's fingerprinting of samples collected from May to September 2010, Paper presented at SETAC North America 31st Annual Meeting, Portland, OR, November 7 – 11 , 2010.

Hach Company, 1992. Water Analysis Handbook. Hach Company, Loveland, Co.

Halihan, T., Paxton, S., McPhail, M., McSorley, H., and Riley, M., 2005a, Final Report for:

Environmental Characterization and Monitoring of LNAPL Using Electrical Resistivity Tomography (ERT) and Hydraulic Push Techniques, Oklahoma Corporation Commission.

Halihan, T., Paxton, S., Graham, I., Fenstemaker, T., and Riley, M., 2005b, Post-Remediation Evaluation of a LNAPL Site Using Electrical Resistivity Imaging, Journal of Environmental Monitoring, v. 7, p. 1−6.

Hazen, T. C., 2011: Oil Biodegradation and Beioremediation, A Tale of the Two Worst Spills in U.S. History: Environ. Sci. Technol. **45**, 6709-6715

Kaufmann, O., and J. Deceuster, 2007, A 3D resistivity tomography study of a LNAPL plume near a gas station at Brugelette (Belgium): Journal of Environmental and Engineering Geophysics, **12**, 207-219.

Kostka. J.E., O. Prakash., W.A. Overholt., S. J. Green., G. Freyer., A. Canion., J. Delgardio., N. Norton., T. C. Hazen, M. Huettel., 2011, Hydrocarbon-Degrading Bacteria and the Bacterial Community Response in Gulf of Mexico Beach Sands Impacted by the Deepwater Horizon Oil Spill. Appl. Environ. Microbiol. **77**, 962–7974

Kvenvolden, K. A., and Cooper, C. K., 2003, Natural seepage of crude oil into the marine environment: Geo-Mar Lett, **23**, 140-146

Le Borgne. S., D. Paniagua., and R. Vazquez-Duhalt**,** 2008, Biodegradation of organic pollutants by halophilic bacteria and archaea. J Mol Microbiol Biotechnol. **15**,74-92

Lisle, J. T., Comer, N. N., 2011, Characterization of sediments from the Gulf of Mexico and Atlantic shorelines, Texas to Florida: Open-File Report. U.S. Geological Survey, no.2011-1199, pp 12

MacDonald, I.R., Reilly, J.F. Jr, Best, W.E., Venkataramaiah , R., Sassen, R., Gusnasso, N.R. Jr, Amos, J., 1996, Remote sensing inventory of active oil seeps and chemosynthetic communities in the northern Fulf of Mexico. In: Schumacher D, Ab rams MA (eds) Hydrocarbon migration and its near-surface expression. Am Assoc Petrol Geol Mem, **66**, 27-37.

MacDonald, I.R., Leiger, I., 2002, Constraining rates of carbon flux from natural seeps on northern Gulf of Mexico Slope. In: Abstr Vol 7th Int Conf Gas in Marine Sediments, 7-12 October 2002, Baku, Azerbaijan. Nafta Press, Baku, pg 119.

Margesin, R., Schinner, F., 2001, Biodegradation and bioremediation of hydrocarbons in extreme environments: Appl Microbiol Biotechnol, **56**, 650-663.

Mazác, O., Benes, L., Landa, I., Maskova, A., 1990, Determination of the extent of oil contamination in groundwater by geoelectrical methods: Ward SH (ed) Geotechnical and environmental geophysics, **2**,107-112

Minsley, B. J., J. Sogade, and F. D. Morgan 2007, Three-dimensional self-potential inversion for subsurface DNAPL contaminant detection at the Savannah River Site, South Caroline, *Water Resour. Res., 43*, W04429, doi:10.1029/2005WR003996.

Natter, M., Keeven, J., Wany, Y., Keimowitz, A. R., Okeke, C. O., Son, A., Lee, M., 2012, Level and Degradation of Deepwater Horizon Spilled Oil in Coastal Marsh Sediments and Pore-Water: Environ. Sci. Technol., **46**, 5744-5755.

Operational Science Advisory Team. 2011. Summary Report for Fate and Effects of Remnant Oil in the Beach Environment. New Orleans: Gulf Coast Incident Management Team. http://www.restorethegulf.gov/sites/default/files/u316/OSAT2%20report%20no%20-ltr.pdf (accessed August 15, 2012)

Pérez-Pantoja. D., B. González., and D.H. Pieper, 2010, Aerobic Degradation of Aromatic Hydrocarbons. p. 799-837. *In* K. N. Timmis (ed.), Handbook of Hydrocarbon and Lipid Microbiology. Springer-Verlag Berlin Heidelberg.

Samouëlian, A., Cousin, I., Tabbagh, A., Bruand, A., Richard, G., 2005, Electrical resistivity survey in soil science: a review: Soil and Tillage Research, **83**, 173-193

Sauck, W. A., E. A. Atekwana, and M. S. Nash 1998, High conductivities associated with an LNAPL plume imaged by integrated geophysical techniques, *J. Environ. Eng. Geophys,*. *2*(3), 203-212.

Sauck, W., 2000, A model for the resistivity structure of LNAPL plumes and theirenvirons in sandy sediments: Journal of Applied Geophysics, **44,** 151-165

Schemel, L.E., 2001, Simplified conversions between specific conductance and salinity units for use with data from monitoring stations: IEP Newsletter, **14**, 17−18

Werkema, D. D., E. A. Atekwana, L. E. Anthony, W. A. Sauck, and D. P. Cassidy, 2003, investigating the geoelectrical response of hydrocarbon contamination undergoing biodegradation: Geophysical Research Letters, **30**, 49-1-49-4.

Whitehouse, B. G., 1984, The effects of temperature and salinity on the aqueous solubility of polynuclear aromatic hydrocarbons: Mar Chem, **14(4)**, 319-332.

Wolfe, M. F., Schwartz, G. J. B., Singaram, A., Mielbrecht, E. E., Tjeerdema, R. S., Sowby, M. L., 1998, Effects of salinity and temperature on the bioavailability of dispersed petroleum hydrocarbons to the golden-brown algae *Isochrysis galbana*: Arch Environ Contam Toxicol, **35**, 268-273.

Yang, L., Lai, C., Shieh, W. K., 2000, Biodegradation of dispersed diesel fuel under high salinity conditions: Wat. Res. V.34, no.13, 3303-3314.

Yang, C. H., C. Y. Yu, and S. W. Su, 2007, High resistivities associated with a newly formed LNAPL plume imaged by geoelectric techniques-A case study: Journal of the Chinese Institute of Engineers, **30**, 53-6

APPENDICES

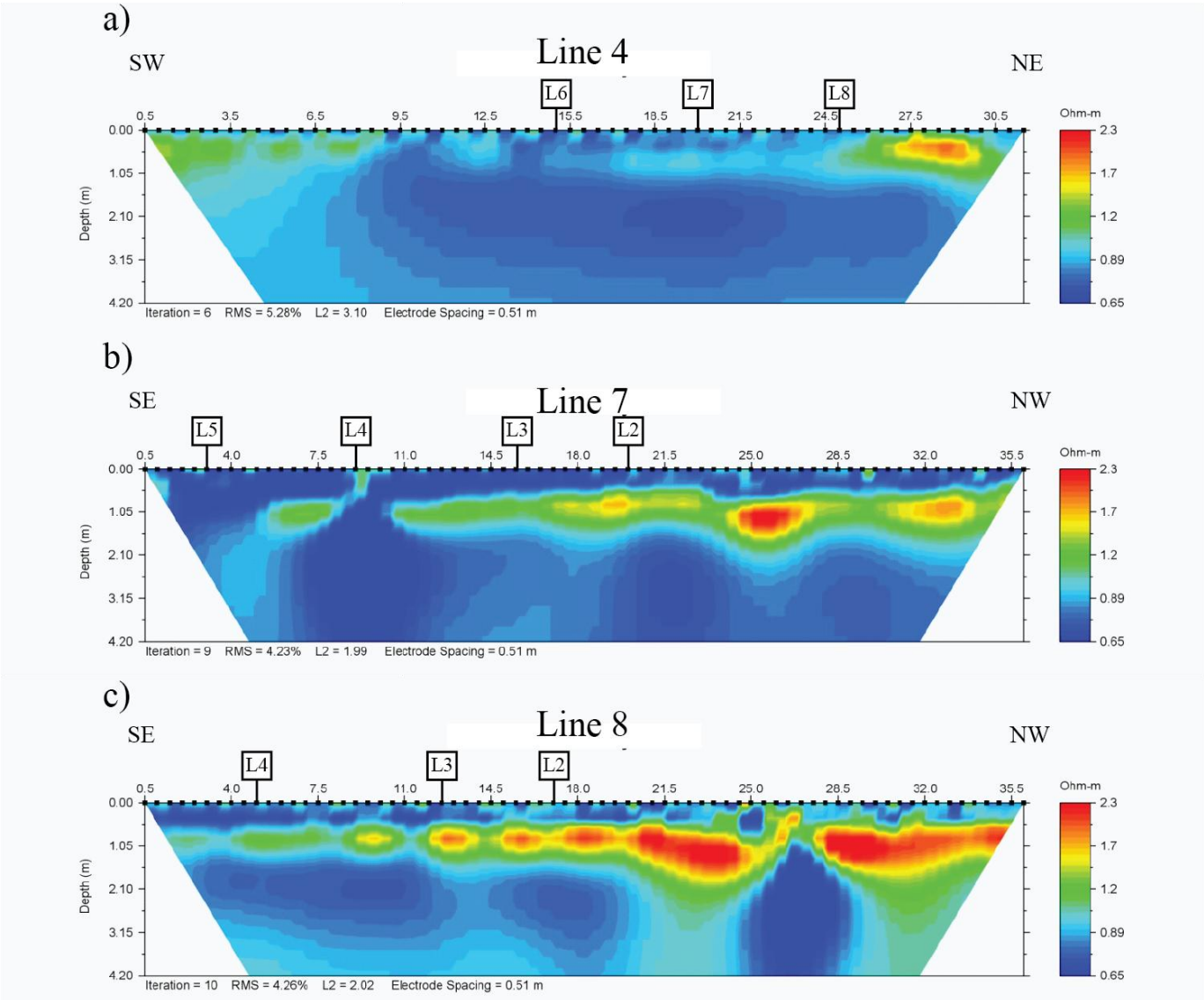

Figure 21 2D electrical resistivity (ER) images of a) L4, b) L7, and c) L8

.

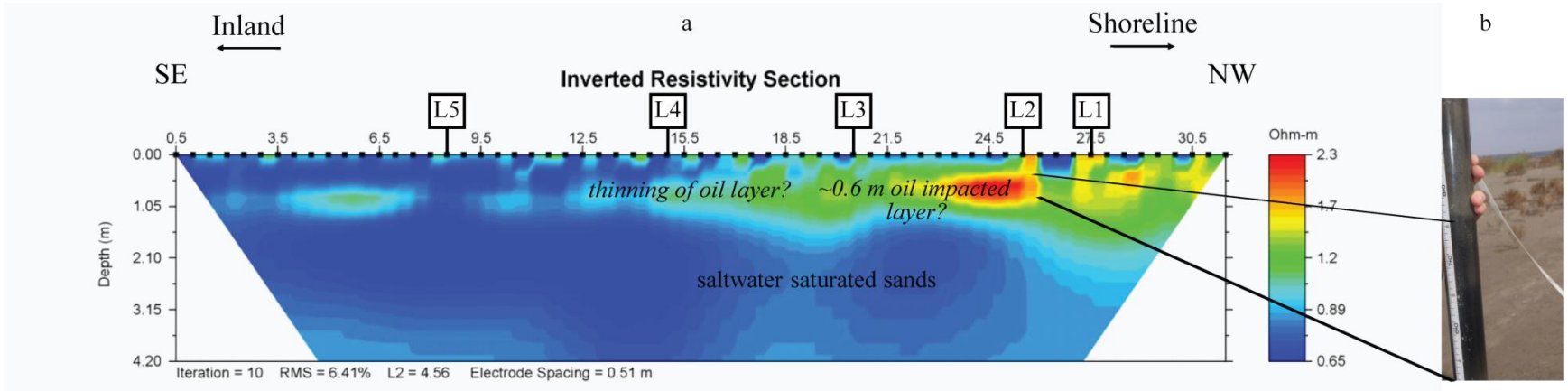

Figure 22. a) 2D apparent resistivity section of line 6 showing the relatively higher resistivity layer, and how it spatially coincides with the b) darkened layer of soil seen in extracted cores from the the area of elevated resistivity.

VITA

Cameron Stuart Ross

Candidate for the Degree of Geology

Master of Science

Thesis: GEOPHYSICAL AND GEOCHEMICAL CHARACTERIZATION AND DELINEATION OF A CRUDE OIL SPILL IN A HIGHLY SALINE ENVIRONMENT

Major Field: Geology

Biographical:

Born Traverse City, Michigan, February 22, 1985 to Mr. and Mrs. Tracy and Judy Ross

Education:

Completed the requirements for the Master of Science in Geology at Oklahoma State University, Stillwater, Oklahoma in May, 2013.

Completed the requirements for the Bachelor of Science in Geology at Grand Valley State University, Allendale, Michigan in April 2009

Experience:
Geologist, Columbine Logging Inc., Midland TX (02/2013-Present)
Student Contractor, Environmental Protection Agency under the supervision of Dr. Dale Werkema and Dr. Estella Atekwana (08/2011-06/2012)
Teaching Assistant, Boone Pickens School of Geology (08/2011-04/2012)
Research Assistant, Boone Pickens School of Geology (08/2010-04/2011)
Geologist, Bay Geophysical Inc., Traverse City, MI (09/2009-07/2010)

Professional Memberships:

Geological Society of America (GSA)
American Association of Petroleum Geologist (AAPG)
Society of Exploration Geophysicists (SEG)
Environmental and Engineering Geophysical Society (EEGS)
Geology Graduate Student Association (GSSA)